Tectonics®

RESEARCH ARTICLE
10.1029/2024TC008488

Key Points:

- The Cenozoic deformation field of the southwestern Tian Shan recorded in intra-montane basins resembles that of the Afghan-Tajik Basin fold-thrust belt and the Pamir
- Basement-rooted faults require a mid-crustal detachment consistent with the spacing between the major intra-montane basins
- The southwestern Tian Shan is part of the deformation field of the Pamir and thus governed by the Indian mantle-lithosphere indenter beneath the Pamir

Supporting Information:

Supporting Information may be found in the online version of this article.

Correspondence to:

F. Trilsch and L. Ratschbacher,
florian.trilsch@gmx.net;
lothar.ratschbacher@extern.tu-freiberg.de

Citation:

Trilsch, F., Ratschbacher, L., Vergés Masip, J., Nakapelyukh, M., Schurr, B., & Gadoev, M. (2025). Southwestern Tian Shan: 1. Deformation of Cenozoic intra-montane basins and intervening basement ranges in front of the Indian mantle indenter. *Tectonics*, *44*, e2024TC008488. https://doi.org/10.1029/2024TC008488

Received 2 JUL 2024
Accepted 14 FEB 2025

Author Contributions:

Conceptualization: Florian Trilsch, Lothar Ratschbacher, Jaume Vergés Masip
Data curation: Florian Trilsch, Lothar Ratschbacher, Mykhaylo Nakapelyukh, Bernd Schurr, Mustafo Gadoev
Formal analysis: Florian Trilsch, Lothar Ratschbacher
Funding acquisition: Lothar Ratschbacher
Investigation: Florian Trilsch, Lothar Ratschbacher, Jaume Vergés Masip, Mykhaylo Nakapelyukh, Bernd Schurr

Southwestern Tian Shan: 1. Deformation of Cenozoic Intra-Montane Basins and Intervening Basement Ranges in Front of the Indian Mantle Indenter

Florian Trilsch[1], Lothar Ratschbacher[1], Jaume Vergés Masip[2], Mykhaylo Nakapelyukh[3], Bernd Schurr[4], and Mustafo Gadoev[5]

[1]Institut für Geologie, und Institut für Keramik, Feuerfest und Verbundwerkstoffe, Technische Universität Bergakademie Freiberg, Freiberg, Germany, [2]Geosciences Barcelona Geo3Bcn - CSIC, Barcelona, Spain, [3]Institute of Geodesy, Lviv Polytechnic National University, Lviv, Ukraine, [4]Deutsches GeoForschungsZentrum GFZ, Potsdam, Germany, [5]Tajik Academy of Sciences, Dushanbe, Tajikistan

Abstract A structural analysis of intra-montane basins establishes the deformation field of the southwestern Tian Shan, that part of the Tian Shan that faces the Pamir and thus the deformation that the Indian mantle-lithosphere indenter beneath the Pamir imposes—northward indentation and westward crustal collapse. Tight-isoclinal footwall synclines in the basins accompany major ~E-striking Cenozoic reverse faults that reactivate Paleozoic ones, separate basement blocks, and accommodated ~N–S shortening and dextral strike-slip faulting. They connect with ~WNW-striking dextral strike-slip faults, and ~ENE-striking thrusts; the latter are confined to the western southwestern Tian Shan. The deformation field resembles that of the Afghan-Tajik Basin fold-thrust belt and mimics in shape the geometry of the intermediate-depth earthquake zone beneath the Pamir that traces the lithospheric delamination zone separating the Indian mantle indenter from Asian lithosphere. The basement-rooted Cenozoic faults require a detachment underlying the southwestern Tian Shan, likely along the brittle-ductile transition, consistent with the regular spacing of the intra-montane basins. This mid-crustal detachment and the shallow evaporite detachment below the Afghan-Tajik Basin may root in a common deeper one, likely along the Moho. As the southwestern Tian Shan is involved in the northward motion and westward collapse of the Pamir, the deep detachment must root in the lithospheric delamination zone of the Pamir. The deep structure of the eastern Tian Shan is different; thus, the detachment underlying the southwestern Tian Shan and Afghan-Tajik Basin must terminate along the eastern margin of the Pamir delamination zone, that is, along the western margin of the Tarim craton.

Plain Language Summary The Tian Shan-Pamir-Tibet-Himalaya mountain belts result from the Cenozoic collision of the Asian and Indian continents. Currently, the Pamir is colliding with the Tian Shan and collapsing westward into its foreland depression, creating the Afghan-Tajik fold-thrust belt. We analyze the structure of intra-montane basins and establish the deformation field of the southwestern Tian Shan, that part of the Tian Shan that faces the Pamir and thus the deformation that the Indian mantle-lithosphere indenter beneath the Pamir imposes—northward indentation and westward crustal collapse. We show that the southwestern Tian Shan is—different from the other parts of the Tian Shan—part of the deformation field of the Pamir. Its faults likely root in a detachment that is connected to the lithospheric delamination zone of the Pamir that separates the Indian mantle indenter from Asian lithosphere.

1. Introduction

The Cenozoic Tian Shan of Central Asia is a result of the India-Asia collision and constitutes Earth's largest active intra-continental mountain belt. Its Paleozoic precursor has attracted attention as the type orogen formed by the amalgamation of subduction-accretion, magmatic-arc, and continental-fragment complexes (e.g., Kröner et al., 2014; Şengör et al., 1993; Windley et al., 2007). The Paleozoic orogen was eroded during the Mesozoic and a low-relief erosional surface existed over ~100 Myr in most of the Tian Shan (e.g., Abdrakhmatov et al., 2001; Morin et al., 2019). A first pulse of deformation/exhumation reactivated the Tian Shan in the late Oligocene-early Miocene (30–20 Ma), but major mountain building commenced in the late Miocene (15–8 Ma; e.g., Abdulhameed et al., 2020; Bande, Sobel, Mikolaichuk, & Acosta, 2017; Bande, Sobel, Mikolaichuk, Schmidt, et al., 2017; De Grave et al., 2011; Glorie et al., 2011; Glorie & De Grave, 2016, 2013; Heermance et al., 2008; Jia et al., 2015; Macaulay et al., 2013, 2014; Rolland et al., 2020; Roud et al., 2021; Yang et al., 2014).

Methodology: Florian Trilsch, Lothar Ratschbacher, Jaume Vergés Masip, Mykhaylo Nakapelyukh, Bernd Schurr
Project administration: Lothar Ratschbacher
Supervision: Lothar Ratschbacher, Jaume Vergés Masip
Validation: Florian Trilsch, Lothar Ratschbacher, Jaume Vergés Masip, Bernd Schurr
Visualization: Florian Trilsch, Lothar Ratschbacher
Writing – original draft: Florian Trilsch, Lothar Ratschbacher
Writing – review & editing: Florian Trilsch, Lothar Ratschbacher, Jaume Vergés Masip, Bernd Schurr

The rise of the Cenozoic Tian Shan—in particular its late Miocene intensification—poses major questions to tectonic research. Among them, the trigger for its major mounting-building phase is likely the most unclear. Models postulated (a) stress transfer from the cratonic Tarim block, with its clockwise rotation causing shortening and minor sinistral strike-slip shear across the eastern Tian Shan—for the purpose of this paper defined as the Tian Shan east of the Talas-Fergana Fault (Avouac et al., 1993; Cui et al., 2024; Yin et al., 1998); (b) collision of the Pamir salient with the western Tian Shan—the Tian Shan west of the Talas-Fergana Fault (Bande, Sobel, Mikolaichuk, Schmidt et al., 2017; Burtman & Molnar, 1993; Thomas et al., 1993). Both models explain aspects (see, e.g., discussion in Bande, Sobel, Mikolaichuk, Schmidt et al., 2017) but—for example—do not explain why the Pamir or the Tarim should drive deformation of the entire Tian Shan synchronously. There has been progress: Abdulhameed et al. (2020) were first to relate the late Miocene growth of the Tian Shan to the northward advancing Indian mantle lithosphere that has been causing forceful delamination and rollback of Asian (Tajik-Tarim) lithosphere since ∼12 Ma (Bloch et al., 2021; Kufner et al., 2016). This scenario of an indenting cratonic Indian mantle lithosphere that stretches from the western end of the Pamir to at least the southern edge of the western Tarim craton in Tibet (Bloch et al., 2021; Rai et al., 2006; Zhao et al., 2010) has gained support from geophysical (W. Li et al., 2022) and numerical modeling results (Huangfu et al., 2021).

Other salient questions regarding the Cenozoic Tian Shan remain partly or unanswered: (a) What is the structural style of deformation? (b) How is strain distributed? (c) Is strike-slip shear playing a role in the overall convergence? (d) How do the current rate and distribution of deformation—measured by GNSS and seismicity—compare to the rates and distribution over geologic time scales? (e) How is the deformation in different parts of the Tian Shan, that is, in the western and eastern Tian Shan as defined above, related to the Indian mantle-lithosphere indenter? Several of these questions were addressed in the western parts of the eastern Tian Shan, herein defined as comprising the Kyrgyz and Kazakh Tian Shan. This region is deforming between the stable Kazakh Platform in the north and the cratonic Tarim Basin in the south. GNSS velocities change from ∼20 mm/yr at the northern Tarim Basin to >1 mm/yr in the Kazakh Platform (Zubovich et al., 2010). GNSS and Quaternary slip rates and earthquake focal mechanisms record thrust and reverse faulting with ∼N–S shortening and minor sinistral strike-slip (Engdahl et al., 2020; Thompson et al., 2002).

The Kyrgyz and Kazakh Tian Shan show a basin and range topography, with ∼E-trending ranges defining fault-bounded blocks of mostly Paleozoic rocks (herein "basement"), separated by in part large basins with thick syntectonic Cenozoic sediments (e.g., Abdrakhmatov et al., 2001; Burtman, 1975; Thompson et al., 2002). The low-relief erosional surface—developed on the highly deformed basement—has been preserved over much of the eastern Tian Shan and was used as a marker for reconstructing the deformation (e.g., Abdrakhmatov et al., 2001). Shortening has been concentrated along major faults, mostly along the intra-montane basin margins, with the intervening 35–80 km-wide blocks showing minor deformation. Typically, most of the active faults underlie the basins as gently dipping splays that are connected with steeply dipping faults below the ranges (e.g., Abdrakhmatov et al., 2001; Goode et al., 2014; Thompson et al., 2002).

This paper aims to address several of the above-posed questions in the southwestern Tian Shan—that part of the western Tian Shan that is located at the junction with the Pamir and the Afghan-Tajik Basin and stretches to the Fergana Basin in the north (Figure 1a). This area faces the Indian mantle-lithosphere indenter underneath the Pamir in its eastern part and is adjoining to the area that comprises the westward collapsing Pamir-Plateau crust inverting the Afghan-Tajik Basin and reactivating the Uzbek Gissar, the southwestern tip of the Tian Shan (Figures 1a and 2a; Gągała et al., 2020; Kufner, Schurr, Ratschbacher, et al., 2018; Metzger et al., 2021; Schurr et al., 2014). Käßner et al. (2016)—studying a part of the southern southwestern Tian Shan—showed that this part is likely involved into the collapse and northwestward motion of crust at the western tip of the India-Asia collision zone (Figure 1a and insert bottom right).

Although still sparsely covered with measurements, GNSS velocities decrease from ∼9 mm/yr at the eastern end of the southwestern Tian Shan—close to the Talas-Fergana Fault—to <2 mm/yr at its western end (Figure 1a), compatible with the paleomagnetically determined anticlockwise rotation of the Fergana Basin (Thomas et al., 1993; Zubovich et al., 2010). GNSS- and interferometric-determined deformation rates also confirm the westward collapse of the Pamir-Plateau crust, with shortening rates decaying westward from ∼15 mm/yr in the Trans-Alai Range of the Pamir front to ∼2 mm/yr in the western Afghan-Tajik Basin. Abrupt ∼6 mm/yr horizontal-rate changes occur across the kinematically linked dextral Ilyak strike-slip fault, bounding the Afghan-Tajik Basin fold-and-thrust belt (FTB) to the north, and the Babatag backthrust, located far west in the belt

10.1029/2024TC008488

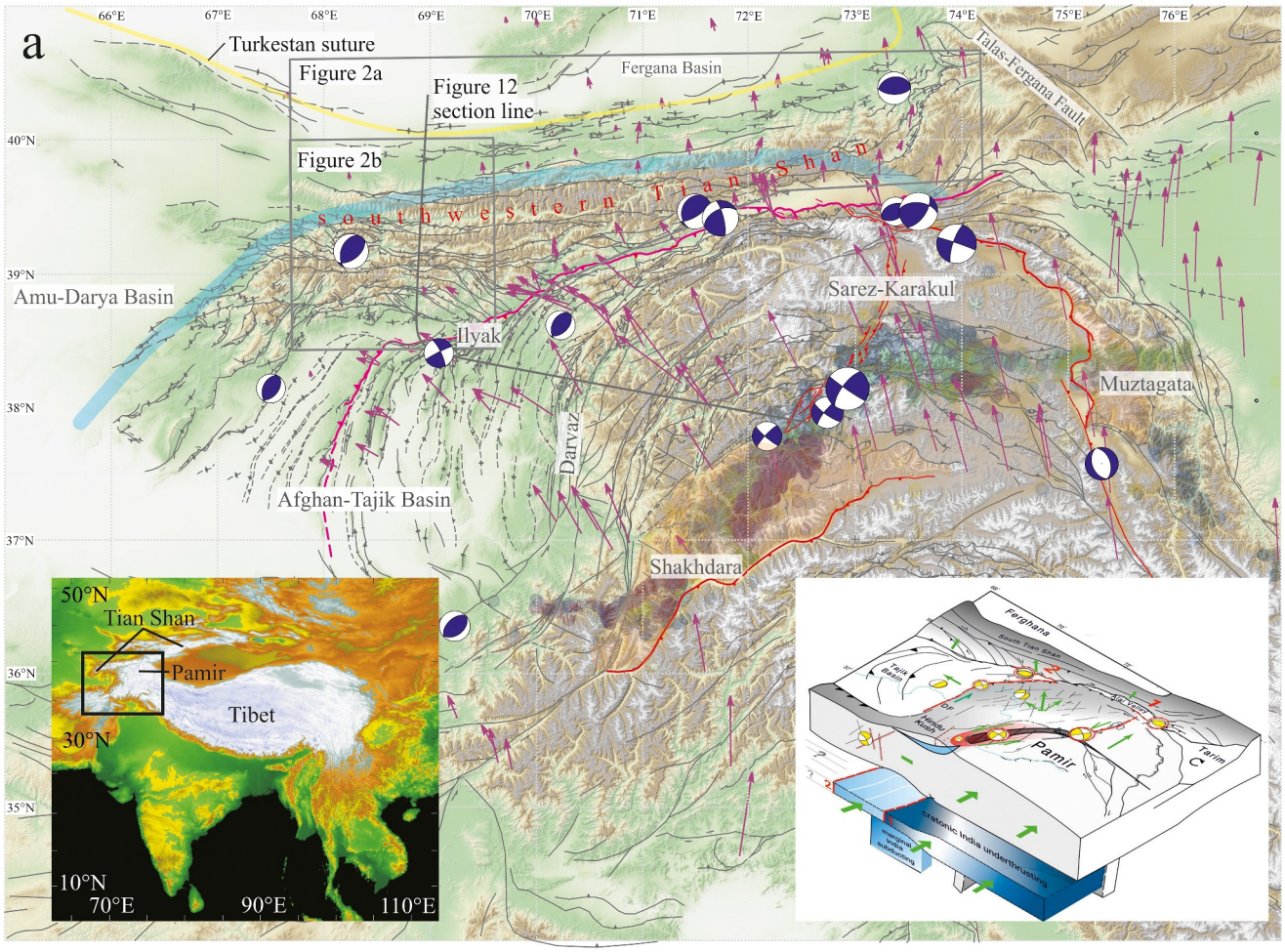

Figure 1.

(Figure 2a for locations; Metzger et al., 2021). Seismicity outlines an east to west change from thrusting to dextral-transpressive strike-slip deformation from the Trans-Alai Range to the fault zones along the Afghan-Tajik Basin's northern and eastern margins (Kufner, Schurr, Ratschbacher, et al., 2018). Within the Basin, seismically derived SH_{max}-axes align with the ~W-trending GNSS-velocity vectors. Seismicity is concentrated in and at the base of a southward deepening, 9–15 km-thick wedge of the Afghan-Tajik Basin FTB. How far the lithosphere underneath the Afghan-Tajik Basin is a rigid block and transfers stress to the southwestern Tian Shan remains unclear: seismicity below the evaporite detachment of the Afghan-Tajik Basin FTB indicates that the sub-detachment crust is involved in the gravitational collapse (Kufner, Schurr, Ratschbacher, et al., 2018) but a few earthquakes indicate that it is also shortening ~N–S (McNab et al., 2019). Seismic activity is much less in the southwestern Tian Shan: the few earthquakes that allow moment-tensor inversions comprise thrust and strike-slip solutions (Figure 1b). Their SH_{max}-axes change trends from northwest in the west to north in the east (Feld et al., 2015; Kufner, Schurr, Ratschbacher, et al., 2018).

In this study, we provide a structural analysis focusing on the intra-montane basins to establish the deformation field of the southwestern Tian Shan. In contrast to the eastern Tian Shan, the ranges of the southwestern Tian Shan expose mostly Paleozoic basement, deficient of markers for separating Paleozoic and Cenozoic deformation and for detailing its spatio-temporal distribution. Mesozoic-Cenozoic strata—capable of unequivocally recording Cenozoic deformation—are preserved in few-km-wide remnant intra-montane basins. The Mesozoic-Cenozoic strata mainly occupy the footwalls of major reverse faults, are often deformed into tight synclines, and can be used to estimate minimum amounts of shortening. In a companion paper, Trilsch, Reuter, et al. (2025) detailed the timing of Cenozoic exhumation and its spatio-temporal variation by thermochronologic methods and used these data to estimate the displacements across some of the reverse faults. They showed that deformation commenced at 15–10 Ma, contemporaneously with the onset of the inversion of the Afghan-Tajik Basin into a FTB (e.g., Abdulhameed et al., 2020; L. Li et al., 2022). We first detail the structure of several of the intra-montane basins along a broad swath over the southwestern Tian Shan by presenting maps, cross sections, and field-based structural measurements. We then trace these structures along-strike to the west (Seven Lakes transect) and east (Garm Massif, Alai Range).

Our work shows: (a) Basement-rooted reverse faults reactivate Paleozoic ones, dominate the structural style, and bound the major basins. While the basin strata absorbed the dominant N–S shortening via large synclines, both the boundary faults and partly newly formed, ~WNW-striking faults accommodated dextral strike-slip deformation. (b) Shortening is concentrated in the central part of the southwestern Tian Shan and diminishes toward north and south. Shortening within individual basins is heterogenous, reaching up to 40%; total shortening across the southwestern Tian Shan amounts to 15–40 km. (c) The deformation field of the southwestern Tian Shan resembles that of the Afghan-Tajik Basin FTB, constituting the northern margin of the crustal section that shortens N–S and extrudes westward from the Pamir. This implies that—in contrast to the eastern Tian Shan—the southwestern Tian Shan and the Afghan-Tajik Basin are underlain by a detachment that roots in the lithosphere-scale delamination zone beneath the Pamir. Thus, the southwestern Tian Shan, the Afghan-Tajik Basin FTB, and the adjacent Pamir form a continuum that has existed since the onset of indentation of the Indian mantle lithosphere into the Asian (Tajik-Tarim) lithosphere.

Figure 1. Cenozoic structures, GNSS velocities, seismicity, and deep structure of the Pamir, Afghan-Tajik Basin, and southwestern Tian Shan. (a) Cenozoic faults and folds (black) mostly interpreted from 1:200.000 and 1:500.000 Soviet-time geologic maps and verified by own field expeditions. GNSS rates with respect to stable Eurasia (Ischuk et al., 2013; Metzger et al., 2020; Mohadjer et al., 2010; Perry et al., 2019; Zubovich et al., 2010, 2016) outline the northward motion and (north)westward collapse of the Pamir-Plateau crust into the Afghan-Tajik Basin. Blue beach balls represent double-couple components of moment tensors for selected crustal earthquakes, deemed representative for the deformation field. Hindu Kush and Pamir intermediate-depth seismicity (color-coded for depth) from Bloch et al. (2021) and Kufner et al. (2017). These earthquakes outline the subducting Indian slab beneath the Hindu Kush in the west. The Pamir earthquakes farther northeast outline the Indian mantle-lithosphere indenter below the Pamir and western Tibet. Inset bottom left shows the location of (a) in the India-Asia collision zone. Inset bottom right is from Kufner, Schurr, Ratschbacher, et al. (2018) and an interpretation of the neotectonics. It sketches the Indian mantle lithosphere at subcrustal depths as light and dark blue bodies (not to scale); the red dashed lines mark the outline of the transfer corridors between the subducting marginal India (Hindu Kush) and the indenting India (Pamir and western Tibet). Yellow focal mechanisms indicate the style of crustal deformation. Green arrows show directions of material flow within the crust imposed by the Indian convergence at subcrustal depths and the gravitational collapse of the western Pamir. Colored lines/bands outline (i) the northern boundary of the southwestern Tian Shan that is affected by the collapse of the Pamir-Plateau crust (according to this study), (ii) the leading active fault zone of the Pamir and the Afghan-Tajik fold-thrust belt (Pamir Frontal Thrust, Vakhsh Thrust, and Ilyak Fault), and the extension structures of the Pamir, active at ≤~13 Ma. (b) Crustal (<50 km) seismicity (dots) color-coded for depth recorded in the TIPTIMON (2012–2014) and TIPAGE (2008–2010) projects. Moment tensors with *P*-axes (black lines) are from Bloch et al. (2023), Feld et al. (2015), and Kufner, Schurr, Ratschbacher, et al. (2018), with size scaled by moment magnitude with minimum and maximum values of 3.0 and 7.2, respectively.

10.1029/2024TC008488

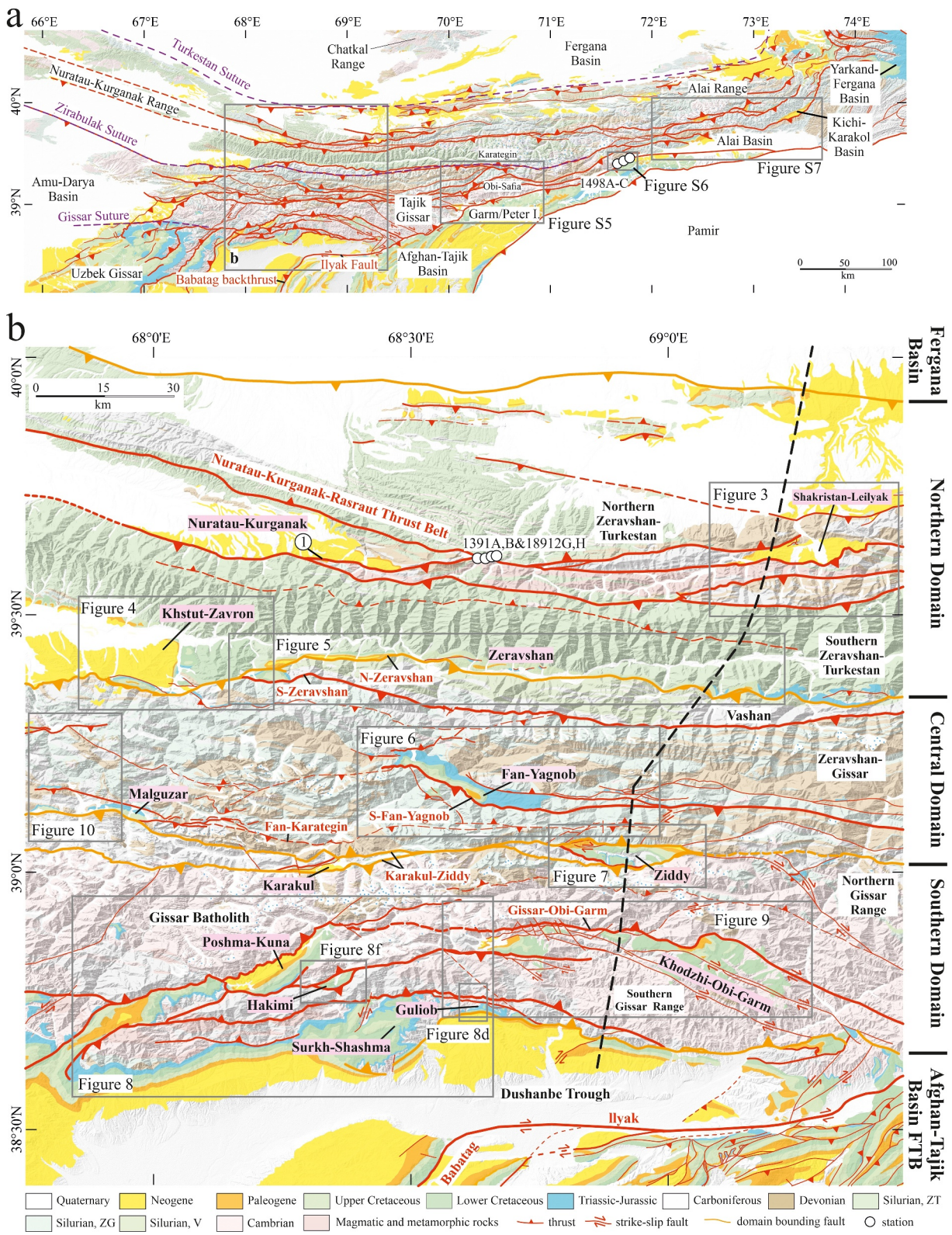

Figure 2.

2. Structural and Stratigraphic Framework of the Southwestern Tian Shan

The southwestern Tian Shan is part of the South Tian Shan (Biske et al., 2021; Brookfield, 2000; Burtman, 2008) with the Turkestan Suture as its northern boundary located within the southern Fergana Basin (Figure 2a). We divided the southwestern Tian Shan into Northern, Central, and Southern Domains (Figure 2b and Figure S1 in the Supporting Information); this is based on Paleozoic geology, Cenozoic structures, and thermochronologic data (Bazhenov et al., 1999; Biske et al., 2021; Brookfield, 2000; Burtman, 2010; Käßner et al., 2017; Konopelko et al., 2017; Leonov, 2005; Portnyagin et al., 1976; Trilsch, Reuter, et al., 2025; Volkova & Budanov, 1999; Worthington et al., 2017). The Northern Domain comprises the Southern and Northern Zeravshan-Turkestan Units, which are separated by the Nuratau-Kurganak-Rasraut Thrust belt. This Domain extends from the N-Zeravshan Fault along the southern margin of the Zeravshan Basin in the south to the Fergana Basin in the north; the N-Zeravshan Fault reactivates the Paleozoic Zirabulak Suture. The Northern Domain contains metamorphic sand-siltstones, platform carbonates, and flysch-type clastic rocks. The Central Domain comprises the Vashan Unit in between the N- and S-Zeravshan Faults and the Zeravshan-Gissar Unit south of it. The Vashan Unit comprises calciferous argillite, jasper, and chert, capped by carbonates. The Zeravshan-Gissar Unit consists of schists—the Yagnob complex—and limestones, abundant in its southern part. The Karakul-Ziddy Fault separates the Central from the Southern Domain. The latter hosts the voluminous Gissar Batholith formed by arc magmatism north of the Gissar Suture. The Gissar-Obi-Garm Fault north of the Khodzhi–Obi-Garm and Poshma-Kuna Basins separates this Domain into the Northern and Southern Gissar Ranges. In the west, the Southern Domain is transitional to the ~NE-trending Uzbek Gissar, a basement-cored FTB that constitutes the foreland backstop to the Afghan-Tajik Basin FTB (Bekker, 1996; Bourgeois et al., 1997; Gągała et al., 2020).

The Mesozoic-Cenozoic basins of the southwestern Tian Shan contain epi-continental to continental deposits and cover the basement with a hiatus and an angular unconformity. Figure 2 locates the major basins. Figure S2 provides their lithostratigraphy. The following overview is based on our field observations and Brookfield and Hashmat (2001), Brunet et al. (2017), Clarke (1984), Dzhalilov et al. (1971, 1982), Fürsich et al. (2017), Kaya et al. (2020), Kazakov et al. (2002), Krymholts et al. (1988), Leonov (2005), Mordvintsev et al. (2017), Morin et al. (2018, 2021), Nikolaev (2002), and Shcherba (1990). Above locally occurring Triassic clastic rocks, Lower-Middle Jurassic alluvial-lacustrine strata contain abundant coal layers. As documented in the Amu-Darya, Afghan-Tajik, and Yarkand-Fergana Basins, the Jurassic sedimentation was controlled by normal faults that caused thickness variations and local non-deposition. Extension ceased at the end of the Middle Jurassic (~160 Ma) and was followed by Late Jurassic and Cretaceous thermal subsidence, coequal with a regional shift to semi-arid conditions at the Middle-Late Jurassic transition; this resulted in the deposition of in part coarse-grained red beds. Upper Jurassic evaporites acted as the décollement of the Afghan-Tajik Basin FTB; they are absent in the intra-montane basins of the southwestern Tian Shan.

During the Lower Cretaceous, enhanced hinterland erosion caused deposition of monotonous red beds in the Afghan-Tajik Basin. At the same time, the Basin expanded northward, incorporating the intra-montane basins. During the Late Cretaceous-late Eocene, the wider Afghan-Tajik Basin was affected by five transgression-regression cycles related to the Proto-Paratethys Sea (e.g., Bosboom et al., 2017; Burtman, 2000; Carrapa et al., 2015; Kaya et al., 2020): shallow marine and clastic continental deposits alternated. A regional marker horizon is the Paleogene Bukhara limestone, a marine carbonate-platform deposit. The Proto-Paratethys Sea retreated at the Bartonian-Priabonian boundary (~37 Ma), possibly linked to a major phase of aridification (Bosboom et al., 2017; Kaya et al., 2019; Wang et al., 2019). Synorogenic deposits—widespread in the Afghan-Tajik Basin—are only locally preserved within the intra-montane basins of the southwestern Tian Shan. Their Formations—although not identical—were correlated with those of the Afghan-Tajik Basin (Dedow et al., 2020; Dzhalilov et al., 1982; Klocke et al., 2017; L. Li et al., 2022; Nikolaev, 2002; Shcherba, 1990). The synorogenic

Figure 2. (a) Simplified Cenozoic fault map with Mesozoic-Cenozoic intra-montane basins of the southwestern Tian Shan west of the Talas-Fergana-Fault and locations discussed in the text. Geology and structure are based on the 1:200.000 Soviet-time maps and reinterpreted based on our field work. Abbreviations in the legend: V = Vashan; ZG = Zeravshan-Gissar; ZT = Zeravshan-Turkestan. (b) Cenozoic fault map of the Tajik southwestern Tian Shan. Geology and structure are based on the 1:200.000 Soviet-time maps, numerous detailed studies (see text for references), and data collected during three field expeditions. The section trace indicates the location of the regional cross-section in Figure 11 and Figure S10. FTB, fold-thrust belt. Figure S1 provides an extended version of this Figure including faults and folds that were potentially formed during the Cenozoic.

deposition started with Late Oligocene red beds and peaked with badly dated Miocene strata—mostly conglomerates.

3. Data and Methods

The Soviet-time 1:200.000-scale geologic maps (GRI, 1961–1984) provided the base for our structural interpretations; however, they contain selected and averaged dip data and often lack detail on the structural geometry in the intra-montane basins. Thus, we provide new maps and cross sections based on new field data, Google Earth® imagery that allowed digitizing outcrop stratification, and thermochronologic and paleotemperature data (Trilsch, Reuter, et al., 2025) that constrain overburden. No borehole or seismic data have been available.

Fieldwork was mainly along traverses across the intra-montane basins. We established the location, geometry, and kinematics of the major deformation zones, documenting structures in "stations"—defined as a single or closely spaced outcrops with a consistent set of structural data—and linked them by mapping along traverses. Figures 3–10 present maps, cross sections, photos of key structures, stereonet plots of structural orientations—in particular of bedding and faults—and sketches of field relations for several intra-montane basins; Figures S3–S8 complete that data set. Figure S9 provides a legend to the stereonet data. We use the terms "brittle" and "ductile" scale-dependent: brittle relates to macroscopic rock failure, ductile denotes structures in which crystal-plastic deformation of minerals prevails. Brittle deformation dominates the Cenozoic deformation in the southwestern Tian Shan. We establish the deformation kinematics using fault-offset markers and shear zones/bands. To understand fault arrays, we applied "stress/strain rate/strain" inversion using fault-striae data, employing the "numeric dynamic analysis" (Spang, 1972), implemented by Sperner and Ratschbacher (1994). Following—for example—Gapais et al. (2000), Twiss (2009), and Twiss and Unruh (1998), we argue that fault-striae data describe permanent deformation over a finite amount of time; thus, we use a strain rate/strain approach. Our goal is to map domains with different deformation style and strain rate/strain orientation (principal axes). We further note that all approaches for the derivation of stress/strain rate/strain orientations from folds/faults and fault-striae data provide quite similar results when done in the same "homogeneous" domain. As these methods average of a finite period of time, in our case 15–10 Ma, they may include block rotations and deformation field inhomogeneities.

Detailing the deformation in the southwestern Tian Shan requires the presentation and discussion of many observations. Therefore, each of the following sections provides descriptions of key stations, that is, "observations." Given the interpretative nature of structural studies and the large number of stations, we combined the observations with their interpretations in the same section; a rigorous separation of observation and interpretation in separate results and discussion chapters would require massive repetition. First, we correlated the Mesozoic-Cenozoic strata across the studied basins (Figure S2). Then, we compiled maps that show the key structures, and cross sections that exploit the surface data and incorporate the thermochronologic and paleotemperature data (see below) via the amounts of exhumation. Cross-section construction used MOVE™ 2022 (Petroleum Experts, UK): we drew a reference horizon constrained by surface data and constructed the other horizons either via the "Parallel" or the "Similar" methods. The first is a kink-bend approach using constant thicknesses, the latter allows thickness changes in different fold parts, as imposed by trishear deformation (Allmendinger, 1998; Erslev, 1991).

The new thermochronologic (zircon and apatite (U-Th)/He, ZHe, AHe; apatite fission track, AFT) and paleotemperature (vitrinite-reflectance) data in the companion paper (Trilsch, Reuter, et al., 2025) provided the following results: (a) A 15–10 Ma onset of shortening/exhumation in the Central and Northern Domains and in the Southern Gissar Range of the Southern Domain, and an onset at 9–7 Ma in the Northern Gissar Range. (b) Minimum or maximum exhumation values, providing lower or upper bounds for the eroded strata. AFT-ages $\leq$~13 Ma indicate exhumation from $\geq$4 km depth; ages >13 Ma that were partially reset within the AFT partial-annealing zone (60–120°C) record 2–4 km or <2 km of exhumation, constrained by thermal history models. Some detrital apatite samples in the footwalls of reverse faults provided both reset and partially reset AFT-age components; the reset components are from F-apatite, with a closure temperature of ~120°C, which corresponds to an exhumation depth of ~4 km. The paleotemperature estimates were converted to overburden using a geothermal gradient of 25°C/km.

The maps of Figure 2 focus on the reliable Cenozoic structures. In contrast, Figure S1 shows all structures that were active or potentially active during the Cenozoic. Reliable Cenozoic structures affect Mesozoic-Cenozoic

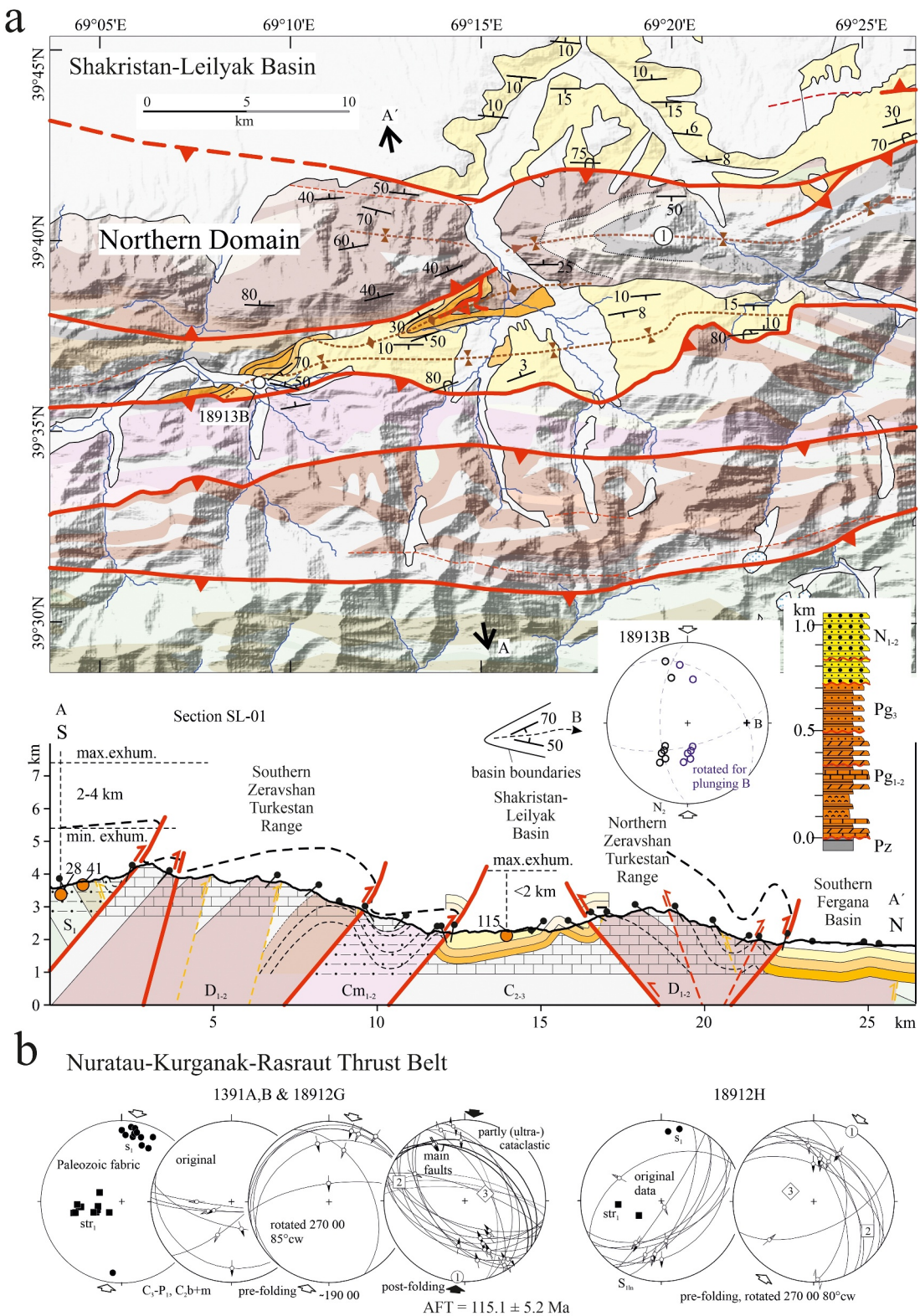

Figure 3.

strata; potentially Cenozoic ones displace younger over older Paleozoic strata, or show opposite vergence within a sequence of consistently verging Paleozoic nappes. For the sections across the intra-montane basins, we calculated the amount of shortening for a specific horizon by line-length restoration; Table 1 provides the results. Due to the lack of geophysical data, the deep structure of the cross sections is conceptual; therefore, we address our regional cross section and regional forward model in the Discussion (Section 5) and Text S1 in Supporting Information S1.

4. Results: Intra-Montane Basin Structure

4.1. Northern Domain: Nuratau-Kurganak-Rasraut Thrust Belt and Nuratau-Kurganak and Shakristan-Leilyak Basins

The Nuratau-Kurganak and Shakristan-Leilyak Basins and basins farther east are within the bi-vergent Nuratau-Kurganak-Rasraut Thrust Belt that separates the Northern and Southern Zeravshan-Turkestan Units (Figures 2a and 2b; Leonov, 2005; Rogozhin, 2004). The thermochronologic data indicate <2 km exhumation in the Nuratau-Kurganak and in the Shakristan-Leilyak Basins. In the Nuratau-Kurganak Basin, Paleogene-Neogene strata form an open syncline (GRI J-42-II map and cross section in Rogozhin, 2004). Its eastward tapering and the steepening of the limbs record eastward increasing shortening. The southern boundary is a top-to-~N reverse fault displacing basement as old as Cambrian onto Pliocene strata; relict Santonian-Paleogene strata in an imbricate in the Basin's SE -corner, where the reverse fault bi-furcates (① in Figure 2b), outline a buried syncline along the southern Basin margin and the presence of a Cretaceous-Neogene Basin fill. The northern Basin contact is transgressive on the here ~15° S-dipping low-relief erosional surface. Locally, Paleogene-Neogene strata dip steeply, indicating Cenozoic displacement along the ~S-vergent northern boundary fault, which mostly runs in basement rocks.

The 5 × 30 km Shakristan-Leilyak Basin (Figures 2b and 3a) contains up to 1,000 m-thick Paleogene-Neogene deposits. The Pliocene (N_2) deposits are mass-flow breccia and conglomerates with some sandstones. The Basin constitutes a syncline; its northern limb dips 10–15° south in the east with Neogene strata lying unconformably on basement rocks. In the western Basin, the northern margin contains an anticline-syncline pair that is cut by a top-to-~S reverse fault. The southern Basin margin is overturned (80–90°) in a ~100 m-wide zone hosting secondary folds. Station 18913B measured in Neogene strata of the westernmost Basin traces a tight syncline with an ~E-plunging axis, cut by the southern boundary fault oblique to its strike. Unfolding the plunging axis suggests pure N–S shortening. Section SL-01 extends beyond the Shakristan-Leilyak Basin highlighting additional features: (a) A top-to-~N reverse fault displaces basement onto openly folded Neogene strata of the Fergana Basin; the footwall strata are overturned. (b) A double-plunging basement syncline (① in the map of Figure 3a), partly cut by a splay of the northern reverse fault, is likely a Cenozoic structure. (c) Reverse faults to the south of the Basin highlight the typical spacing of the faults in the Northern Domain, which is less than in the Central and Southern Domains; this spacing estimate is based on relict Mesozoic-Cenozoic strata and the number of faults per unit length that place younger over older Paleozoic strata.

The stations of Figure 3b (1391A, B, 18912G, and 18912H, location Figure 2b) characterize the Nuratau-Kurganak-Rasraut Thrust Belt, in particular the northern boundary fault of the Nuratau-Kurganak and Shakristan-Leilyak Basins. Silurian metasiltstones with dolerite dikes thrusted top-to-~S onto Pennsylvanian marble conglomerate. The fault zone shows (ultra-)cataclasites and black clay-gouge with up to cm-sized gypsum crystals. The Paleozoic foliation (s_1) is subvertical with a steeply plunging mineral lineation (str_1) in a tightly folded sequence in the fault's hanging wall. The fault zone contains a pre-folding fault set with apparent dextral strike-slip and normal faults that upon unfolding of s_1 are top-to-~S thrusts. The post-folding set comprises dextrally oblique reverse faults that commonly reactivate s_1; the main faults dip steeply NE.

Figure 3. (a) Map, cross section, and stratigraphic column of the Shakristan-Leilyak Basin region, representative for the Northern Domain. The top of the Pg_{1-2} horizon was used for line-length restoration. Labeled arrows (A–A′) indicate the section trace. Dashed lines indicate minimum and maximum exhumation determined from thermochronology (apatite fission track data; the ages are given as numbers (in Ma) and are color-coded for age ranges, following Trilsch, Reuter, et al., 2025). The stereoplot and the sketch characterize the tight syncline in the westernmost Basin and its ~E-plunging axis. Abbreviations in the stratigraphic column: N_{1-2} = Miocene-Pliocene; Pg_{1-2} = Paleocene-Eocene; Pg_3 = Oligocene; Pz = Paleozoic. (b) Structure of the northern boundary fault of the Nuratau-Kurganak and Shakristan-Leilyak Basins measured in the central Nuratau-Kurganak-Rasraut Thrust Belt (stations located in Figure 2b). Abbreviations: C_{2-3} = middle-upper Carboniferous; Cm_{1-2} = lower-middle Cambrian; D_{1-2} = lower-middle Devonian; S_1 = lower Silurian. See Figure S9 for a legend to the stereoplots.

10.1029/2024TC008488

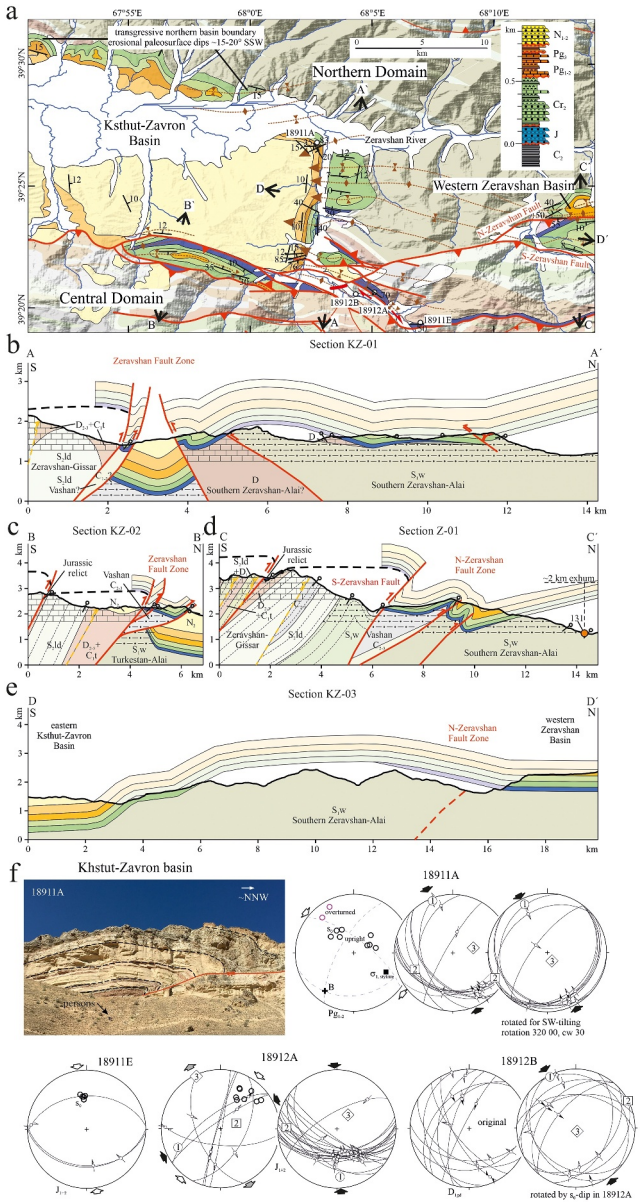

Figure 4. (a) Map and stratigraphic column of the eastern Khstut-Zavron and western Zeravshan Basins along the border of the Central and Northern Domains. (b)–(e) Cross sections (traces in panel (a)). Line-length restoration was performed for the top of the Cr_2–Cm–T horizon for Sections KZ-01 and Z-01. (f) Upper panel: outcrop image and structural analysis of the thrusted fault-propagation fold in the northeastern corner of the Khstut-Zavron Basin. Lower Panel: structures in the southeastern corner of the Khstut-Zavron Basin, documenting a ~NW-striking dextral-transpressive transfer zone between ~E-striking reverse fault-zone segments. Abbreviations see Figure 3; C_{1-2} = lower-middle Carboniferous; Cr_2–Cm–T = upper Cretaceous, Cenomanian-Turonian; D = Devonian; $D_{2-3} + C_1t$ = middle-upper Devonian and lower Carboniferous, Tournaisian; N_2 = Pliocene; S_1w = Wenlock; S_2ld = Llandovery; $S_2ld + D_1$ = Llandovery and lower Devonian.

4.2. Domain Divide: Khstut-Zavron and Zeravshan Basins Along the Boundary Between the Northern and Central Domains

With along-strike discontinuities, these basins stretch across most of the southwestern Tian Shan (Figure 2b). They are in the footwall of the N-Zeravshan Fault that reactivated the Paleozoic Zirabulak Suture (Brookfield, 2000) and separates the Southern Zeravshan-Turkestan Unit of the Northern Domain with 2–4 km exhumation from the Vashan and Zeravshan-Gissar Units of the Central Domain with >4 km exhumation (Biske et al., 2021; Trilsch, Reuter, et al., 2025). Of all intra-montane basins, the Zeravshan Basin has the lowest thickness of Mesozoic-Cenozoic strata (<1,000 m; Figures 4a and 5a, and Figure S2). The N- and S-Zeravshan Faults merge at the western tip of the Zeravshan Basin.

Section KZ-01 (Figure 4b) across the easternmost Khstut-Zavron Basin shows ~700 m shortening over a series of synclines and anticlines that become more open northward; the offsets along associated faults also decrease. The bi-vergent faults of the Zeravshan Fault Zone absorbed most of the shortening. Section KZ-02 (Figure 4c) shows two synclines at the southern Basin margin: the tight southern syncline contains Jurassic strata, the northern one is open. These synclines may indicate the presence of other folds along the southern Basin margin, buried by the hanging wall of the ~N-vergent southern boundary fault. Transgressive Pliocene (N_2) strata on basement of this hanging wall showcase that a major proportion of Cenozoic shortening/exhumation was pre-Pliocene; this is also indicated by the unconformity between Pliocene and Oligocene-Miocene strata and the gentle folding of the Pliocene strata within the Khstut-Zavron Basin.

Jurassic-Cretaceous strata crop out between the N- and S-Zeravshan Faults only at the western tip of the Zeravshan Basin, where the offset along the N-Zeravshan Fault is lowest (~1 km). Section Z-01 (Figure 4d) shows that isoclinal to tight, ~N-vergent anticline-syncline pairs with in part overturned limbs trace the N-Zeravshan Fault zone. A broad syncline and a morphologic plateau characterize the S-Zeravshan Fault footwall. South of the S-Zeravshan Fault, a narrow but >20 km-long string of Jurassic strata occupies the footwall syncline of another ~N-vergent reverse fault; the elevation difference between this Jurassic relict and that north of the S-Zeravshan Fault indicates ~1.5 km vertical offset along the latter, assuming the basement behaves as a rigid block.

Section KZ-03 (Figure 4e) runs ~E-W (along-strike) across the basement that separates the Khstut-Zavron and Zeravshan Basins. It showcases folding of the base of the Mesozoic strata with ~N-trending fold axes that are about normal to the dominant ~E-trending ones. Stations 18911A (Figure 4f) at the northeastern corner of the Khstut-Zavron Basin highlights that inference. A ~100 m-scale thrusted fault-propagation fold in Paleocene-Eocene strata has a partly overturned hanging-wall anticline with ~50 m offset. Shortening, determined from oblique stylolites in limestone along the ramp, is NW–SE. The fold axis, the thrust, and most of the secondary faults plunge/dip ~30° SW, consistent with the ≤45° west-dip of the eastern Basin margin. Unfolding results in a pure thrust solution with NW–SE shortening and shows that the SW tilt mostly post-dates the fault-propagation fold formation.

Stations 18911E to 18912A, B (Figure 4f) detail structures southeast of the Khstut-Zavron Basin, where the regional ~E strike of the reverse faults

10.1029/2024TC008488

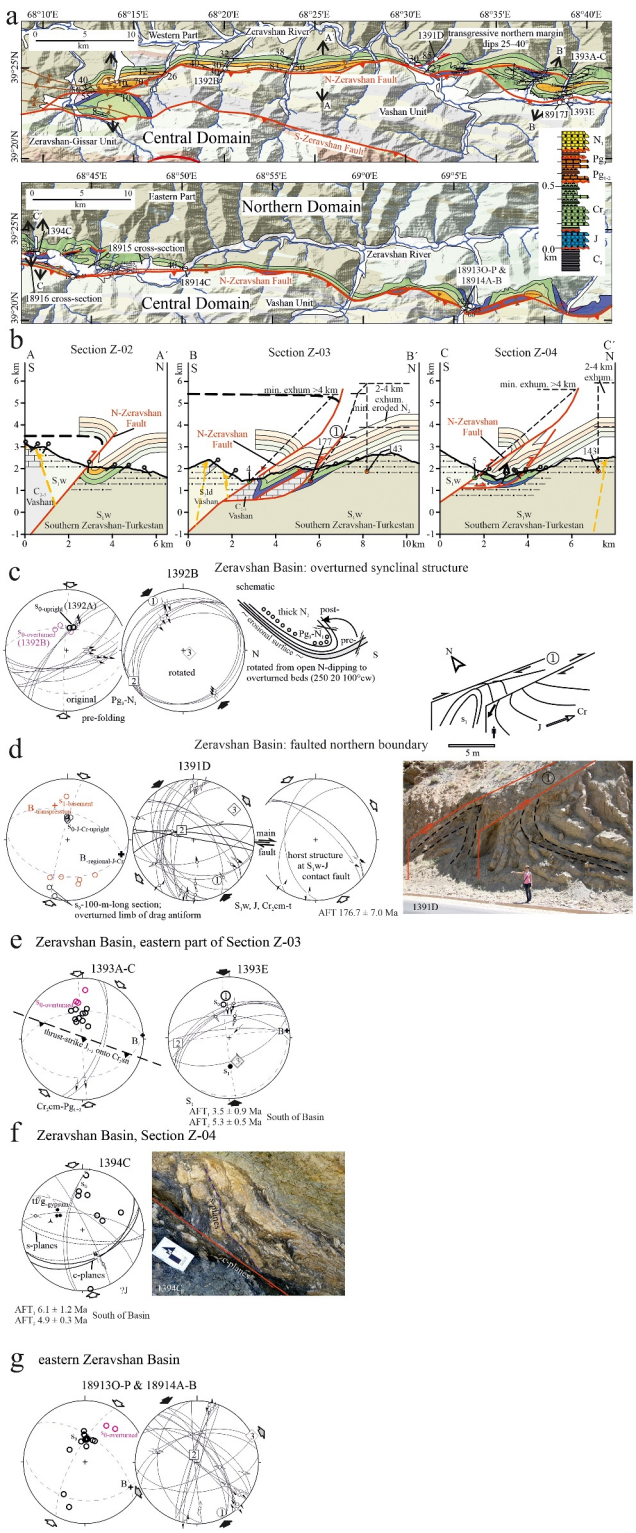

Figure 5.

changes locally to ~NW (Figure 4a), a feature that we observe throughout the southwestern Tian Shan. Faults in station 18911E in the Jurassic footwall-syncline relict strike ~E and bedding dips steeply south along with the regional fault trend. This trend changes to ~NW and bedding dips ~SW in the same footwall syncline at station 18912A. A first fault set has mostly strike-slip faults with ~NNE–SSW shortening, similar to that deduced from bedding orientation. The second set records oblique-slip thrusts with ~N–S shortening, reactivating bedding in a dextral strike-slip zone; the first set may have been rotated clockwise in this fault zone. Station 18912B in basement limestones—farther west outside the dextral fault zone—shows ~NNW–SSE shortening.

The Zeravshan Basin records the highest amount of internal deformation among the basins of the southwestern Tian Shan. It narrows eastwards, recording an eastward increase of shortening, consistent with eastward younging AFT ages (Trilsch, Reuter, et al., 2025), and higher shortening (18%–31%) than in the eastern Khstut-Zavron Basin (~5%; Figure 5a). Its structure varies from a syncline with ~1 km shortening (Section Z-02) to a fold-thrust stack with ~2.5 km shortening (Sections Z-03 and Z-04; Figure 5b). In general, the Basin's southern margin is a 30–45°-dipping reverse fault—the N-Zeravshan Fault—accompanied by a footwall syncline with overturned strata, locally dipping as shallow as 30–40°. The main detachment for the thin-skinned, Basin-internal folds is the basement-cover boundary. At the northern boundary, the Basin strata transgress on the regional low-relief surface, here cut into Silurian meta-clastic rocks (Figures S3a and S3b), which dips 30–40° south, steeper than the ~15°-dip north of the Khstut-Zavron Basin. Horizontal Holocene strata cover wide areas of the Zeravshan-Basin strata along an angular unconformity, suggesting that the N-Zeravshan Fault is currently inactive or accommodates low strain (Figures S3b and S3c).

In Section Z-03 (Figure 5b), the southern reverse fault—the N-Zeravshan Fault—is covered by Holocene strata; the tight to partly overturned syncline is projected from the east, where the syncline-core beds are strongly thickened. West of this Section—where the fault strikes NW—the N-Zeravshan Fault obliquely cuts ~S-dipping strata without a syncline. Farther NW along Section Z-03, a tight anticline and a top-to-~NNW fault that thrusts basement onto Santonian strata without an accompanying fold follow. Section Z-04 (Figure 5b) shows a sequence of three syncline-anticline pairs with ~2.5 km of shortening, the maximum value in the Zeravshan Basin.

Figure 5. (a) Map and columnar stratigraphic section of the Zeravshan Basin at the divide between the Central and Northern Domains. (b) Cross sections (traces in panel (a)) showing fold-fault sequences in the Mesozoic-Cenozoic basin strata. Line-length restoration was performed for the top of Pg_{1-2} (Section Z-02) or Cr_2-Cm-T (Sections Z-03 and Z-04) horizons. (c) Structure in the Basin syncline west of Section Z-02. The oblique-slip normal faults are pre-folding and overturned; local overturning explains the thick Neogene strata by doubling in the syncline core. (d) Structures of a faulted northern boundary section of the Zeravshan Basin. (e) Structures parallel to Section Z-03, documenting dextral-oblique slip along a Basin-internal reverse fault (station 1393A-C) and a small pop-up structure just south of the N-Zeravshan Fault (1393E). (f) S-c fabric in gouge (station 1394C) developed in a Basin-internal fault zone. (g) Structures at stations sampled along a ~NW-striking section in the eastern Zeravshan Basin. Abbreviations see Figures 3 and 4.

Station 1392B characterizes the synclinal structure of the Zeravshan Basin in a valley west of Section Z-02 (Figures 5a and 5c). Here, the northern transgressive margin dips 30–40° south. To the south, we measured oblique-slip normal faults in Paleogene-Neogene strata. We interpret the set as pre-folding and the bedding (s_0 ~ 160 30) as overturned, because rotation to an initially shallowly N-dipping bedding transfers the set into one with ~NNW–SSE shortening, compatible with other Zeravshan stations. Overturning also explains the thick Neogene strata by doubling in the syncline core (Figure 5c). At station 1391D, the in general transgressive contact of Mesozoic strata on Paleozoic basement along the northern Basin margin is faulted (Figures 5a and 5d). Dextral-transpressive faulting built a fold, bounded by oblique-slip normal faults, which extruded the fold sub-vertically as a horst in the contact zone between Silurian and Jurassic-Cretaceous rocks. The Jurassic rocks occupy a ~100 m-long zone with an unusual ~N dip. In the gypsum-bearing Upper Cretaceous beds farther south, s-c fabrics indicate top-to-~N shear. Also in this part of the Basin, horizontal Holocene strata cover the older rocks (Figure S3b).

Stations 1393A-C and E accompany Section Z-03 in the valley to its east (Figures 5a, 5b, and 5e). At 1393A, Cenomanian-Turonian red clay with conglomerate cover the low-relief erosional surface; bedding dips ~25° south and steepens to ~50° southward. Still farther south, stations 1393B and C sample the near-field of the reverse fault and associated anticline in Section Z-03 (point ① Figure 5b). The anticline is tight and is accompanied by secondary faults that generally propagate out of folds too small to draw in Section Z-03. The reverse fault at ① strikes ~WNW, oblique to bedding, and together with tear faults indicates ~NE–SW shortening, oblique to that deduced from bedding (Figure 5e); this may indicate dextral transpression along the fault. In the N-Zeravshan Fault footwall, we observed the syncline characteristic for most parts of the Basin. Just south of it, at station 1393E (Figure 5e), top-to-~S backthrusts in basement rocks form together with the N-Zeravshan fault a small pop-up. At close-by basement station 18917J, an AFT-age of ~4 Ma indicates >4 km exhumation across the N-Zeravshan fault; given a dip of 40°, the displacement along the fault is >6 km.

Section Z-04 shows at least two Zeravshan-Basin-internal imbrications with detachments at the base of the Jurassic strata (Figure 5b). The s-c fabric in the gouge of station 1394C (Figure 5f) developed in the fault zone that thrusts Jurassic over Upper Cretaceous (Cr_2) strata in the middle of the section; the Cr_2 strata contain gypsum that migrated to fill tension gashes/fractures in the gouge. Stations 18914C, 18915, and 18916 integrate structural data collected across parts of the Zeravshan Basin east of Section Z-04 (Figures 5a and Figure S3d). They highlight the following features: (a) Bedding occupies great-circle distributions documenting tight-isoclinal folds. Their fold axes plunge ~WSW, indicating axis-parallel culminations and depressions. (b) Faults formed prior to folding are normal; their unfolding yields shortening solutions. (c) Post-folding faults are either conjugate strike-slip faults formed under ~N–S shortening or mostly dextral strike-slip faults. Shortening directions calculated from these sets vary by 30°, which indicates vertical-axis rotations consistent with the strike-slip shear.

Stations 18913O-P and 18914A-B sample a traverse in the eastern Zeravshan Basin (Figures 5a and 5g). The ~NW-strike of bedding in this traverse differs from the general strike but is typical for several parts of the eastern Zeravshan Basin; the bedding distribution indicates ~NE–SW shortening by tight folds. In contrast, the conjugate faults—mostly post-folding and with the dextral set dominating—record NNW–SSE shortening, similar to most parts of the Zeravshan Basin; the wide strike range of these faults indicates formation during vertical-axis rotation under dextral strike-slip, likely also responsible for the unusual-striking sections.

4.3. Central Domain Interior: Fan-Yagnob Basin

The Fan-Yagnob Basin lies in the center of the Zeravshan-Gissar Unit, thus unlike other intra-montane basins not along the boundary between Paleozoic blocks (Figures 2b and 6a). Its >2 km-thick Triassic to Neogene strata exceed those in the other intra-montane basins; the unusually thick Jurassic strata (300–1,000 m) thin northwestward (Leonov, 2005; Shcherba, 1990). Upper Oligocene-Miocene syn-orogenic strata occupy a synclinal core in the east-central Basin.

Section FY-01 (Figures 6a and 6b) highlights syncline-anticline pairs in the western Basin. In the south, the Basin-bounding, top-to-~N S-Fan-Yagnob Fault dips ~50°. The Jurassic strata in its footwall are overturned. A top-to-~S reverse fault—the N-Fan-Yagnob Fault—forms the northern boundary in the western and eastern Basin; in the central Basin (Section FY-02; Figure 6b), transgressive Jurassic strata dip ~40° south. Sections FY-02 and FY-03 across the central Basin outline a syncline (Figure 6b), similar to the weakly shortened parts of the Nuratau-Kurganak, Shakristan-Leilyak, and Zeravshan Basins. The southern limb is typically overturned, the

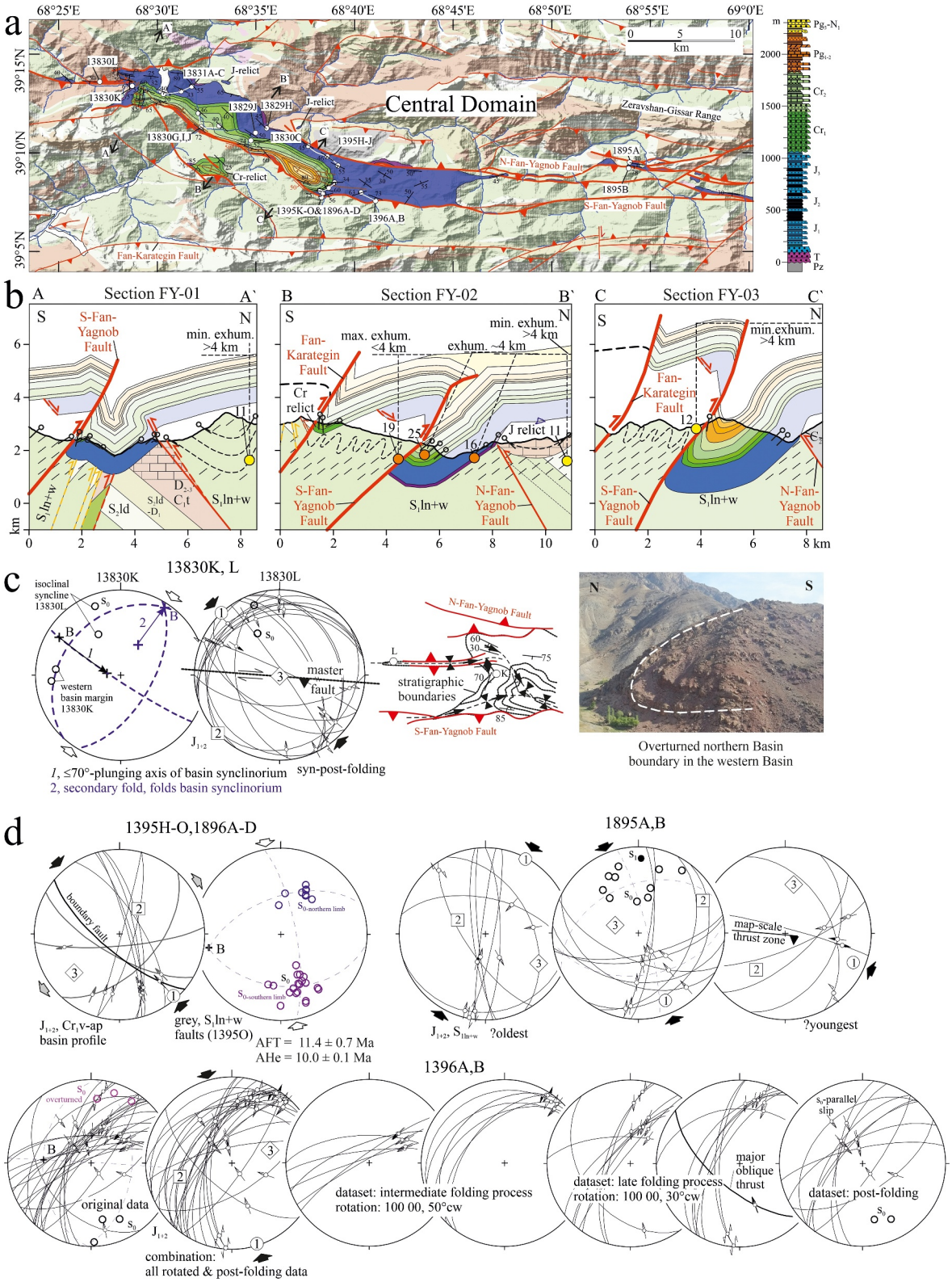

Figure 6. (a) Geologic map of the Fan-Yagnob Basin in the center of Central Doman's Zeravshan-Gissar Unit. Note its position along a step-over between ~E-striking reverse faults. (b) Cross sections (traces in panel (a)). Line length restoration was performed for the top of the Jurassic. (c) Structures at and sketch of the western Basin margin, recording its strongly E-dipping/plunging structural elements. The outcrop image shows the locally overturned northern Basin margin. (d) Structures sampled along traversers in and east of the Fan-Yagnob Basin. Abbreviations see Figures 3 and 4.

northern one dips 25–65°, mostly 40–45°. Section FY-02 crosses Triassic and Cretaceous strata located ∼2 km south of the central Basin. This erosional remnant quantifies the vertical offset across the S-Fan-Yagnob Fault to ∼2 km. The absence of Jurassic strata in the remnant implies their pinch out south of the Fan-Yagnob Basin margin, which we interpret as a result of a top-to-∼N normal fault, fitting the documented Jurassic extension in the western Tian Shan. Along the remnant's southern margin, the strata are overturned and—as the main Basin—bounded by a top-to-∼N reverse fault (Figure S4a). Along strike, this and secondary faults offset younger over older Paleozoic strata, suggesting that they connect to the Fan-Karategin Fault (Figures 2b and 6a; Worthington et al., 2017) and that the latter was reactivated in the Cenozoic. Small remnants of Jurassic strata also crop out north of the Fan-Yagnob Basin. The one projected into Section FY-02 indicates that the strata bend to sub-horizontal close to the northern Basin margin (Figure 6b).

Shortening estimates for the internal deformation of the Fan-Yagnob Basin are 1–2 km (15%–28%; Table 1). AFT ages and paleotemperature estimated from Cretaceous strata within the Basin and the adjacent basement constrain exhumation to ≥4 km north of the Basin and to ∼4 km—thus to only little less—in the central Basin. AFT ages in the S-Fan-Yagnob Fault hanging wall vary along strike, indicating higher exhumation in the east (Section FY-03) than west (Section FY-02; Figure 6b), consistent with the presence of the relict Mesozoic strata south of the central Basin.

The structure of the Fan-Yagnob Basin was studied in a reconnaissance way by Käßner et al. (2016). We integrate their stations (13830A-F, G, I, J, L) with ours. Stations 13830K, L at the western end of the Fan-Yagnob Basin showcase secondary folds and fold interference. At 13830L, a sliver of Jurassic strata forms a tight-isoclinal syncline with a locally overturned or steeply S-dipping northern limb, in part transgressive on basement. A top-to-∼N reverse fault bounds the southern limb. The thrusted syncline interferes with several secondary folds at the western Basin margin, where both bedding and the fold axes dip/plunge ≤70° to the east (station 13830K; Figures 6a and 6c). These folds, all sub-parallel to the main ∼NW-trending basin syncline, were refolded by ∼NNE-trending folds that cause the dip/plunge at the western margin. The 13830K stereoplot shows the measured variation in the plunge of the two fold sets. The interference pattern suggests a strong strike-slip component in the overall deformation, causing rotation of the structural elements out of horizontal positions. The faults at station 13830L, interpreted as syn-to post-folding due to their orientation variation, show ∼NW–SE shortening under dextral transpression, supporting this interpretation.

Stations 13829H, J, 13830C, G, I, J, and 13831A-C characterize the west-central Basin (Figure S4b). Here, the northern Basin boundary is transgressive. Common to these stations are: (a) The S-Fan-Yagnob Fault dips ∼45° SW and its footwall syncline has an overturned southern limb; (b) bedding orientations indicate ∼NE–SW shortening; (c) two fault sets occur: one has thrusts with ∼NE–SW shortening as that deduced from bedding, the other strike-slip faults and ∼NW–SE shortening. Both sets have the same fault characteristics—calcite-fibers—but no age relationship, thus likely formed in a permutating deformation field. Stations 1395H-O and 1896A-D sample a traverse across the east-central Fan-Yagnob Basin, roughly coinciding with Section FY-03 (Figures 6a and 6d). In contrast to the west-central Basin, bedding indicates ∼N–S shortening; associated conjugate strike-slip faults indicate ∼NW–SE shortening. The fold axis of the major Basin syncline plunges west, opposite to that at the western Basin margin, highlighting the depression along the syncline axis, in which the Cretaceous-Neogene strata are preserved. Stations 1396A, B farther SE showcase faulting during progressive fold tightening, thus mostly syn-folding faulting, which produced the wide fault-dip and striae-orientation ranges. The two major sets indicate sinistral-transpressive and thrust kinematics, both with ∼NNW–SSE shortening. Bedding in this eastern part of the Basin is mostly sub-vertical and indicates ∼N–S shortening, similar to the fault-derived shortening.

The eastern and western continuation of the S- and N-Fan-Yagnob Faults in the uniform basement rocks is hard to trace (Figure 6a). Strings of relic Jurassic strata crop out along these Faults in the east and allow the tracing of the Fan-Yagnob Fault System far beyond the Basin (Figure 2). Stations 1895A, B characterize the N-Fan-Yagnob Fault east of the Fan-Yagnob Basin in both basement and Jurassic strata (Figures 6a and 6d). Bedding dips steeply south and shows a wide orientation range; both bedding and oblique-slip faults indicate ∼NNW–SSE shortening. The wide bedding range is reflected by two addition fault sets: the likely younger one with ∼WNW–ESE shortening would impose a dextral strike-slip component on the map-scale fault; the likely older set indicates ∼NNE–SSW shortening. We interpret this set as rotated in the dextral-transpressive fault zone.

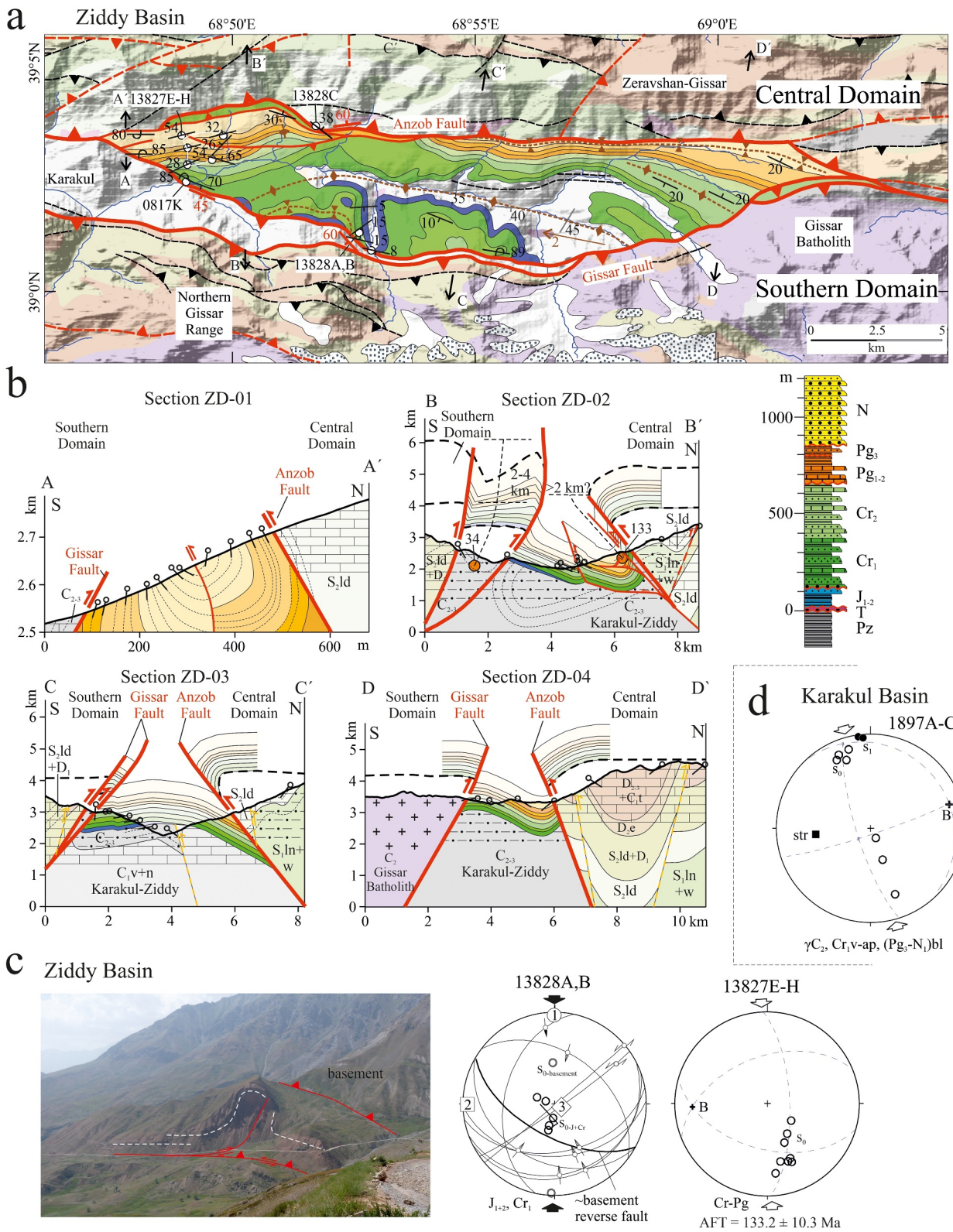

Figure 7.

4.4. Domain Divide: Ziddy and Karakul Basins Between Central and Southern Domain

The Ziddy and Karakul Basins are located between the Southern and Central Domains, that is, between the Zeravshan-Gissar Unit in the north and the Northern Gissar Range in the south (Figure 2b). Opposite-facing, 50–70°-dipping reverse-fault systems bound the Basins, that is, the ∼N-vergent Gissar Fault in the south and the ∼S-vergent Anzob Fault in the north, both constituting the Karakul-Ziddy Fault System (Figure 7a; Kazakov et al., 2002; Leonov, 2005). This fault system can be traced along strike over >300 km and, for example, bounds the basins of the northern Garm Massif farther east. The up to 1,000–1,200 m-thick Mesozoic-Cenozoic strata have 200–350 m-thick syn-orogenic red beds.

Morphologically, the Ziddy Basin occupies a valley. The topography of the surrounding ranges—exposing basement—provides a minimum vertical offset of ∼2.5 km for both the Anzob and Gissar Faults. The Ziddy River cuts through the Mesozoic-Cenozoic sequence and exposes the low-relief erosional surface that forms a gentle anticline (Figure 7a). The surface is ∼1.5 km higher in the eastern than in the western part of the Basin, implying a ∼W-plunging anticline axis (Kazakov et al., 2002). The Ziddy-Basin strata are less deformed than those of the northern basins. Only the westernmost Basin, where the bounding faults merge, exposes a narrow syncline with overturned limbs (Figure 7b; Section ZD-01, modified from Chedia, 1972; Klebelsberg, 1922). An open syncline is the main structure at the Basin's southern margin (Section ZD-02); the southern limb dips gently north, only locally overturning in the west (station 0817K; Käßner et al., 2016). Section ZD-02 crosses along its northern part a ∼100 m-scale, ∼N-vergent anticline in Oligocene-Miocene conglomerates that occupies a triangle structure (Figure 7c); a local detachment lies in upper Paleogene shale and gypsum (Kazakov et al., 2002). Shortening is ≤900 m in the western basin, otherwise ∼300 m (Table 1). Section ZD-03 crosses the central Basin and shows that the here narrow southern syncline transitions into a broad open anticline (0–15° limb dips); its northern limb dips toward the Anzob Fault (30–40° in the western and eastern Basin) or transitions into a narrow syncline (Figure 7b; Section ZD-04, modified from Nesmeyanov & Barkhatov, 1978).

The Anzob Fault is locally accompanied by ≤100 m-thick basement cataclasites (Leonov, 2005; station 13828C of Käßner et al., 2016). Station 0817K of Käßner et al. (2016) characterizes basement imbricates, steeply ∼SW-dipping bedding, and a component of dextral strike-slip at the southwestern Basin margin (Figure 7a). At stations 13828A, B (Figure 7c), vertical basement overthrusts top-to-∼N sub-horizontal Jurassic strata along the ∼60°-dipping Gissar Fault south of a coal mine; secondary faults are mostly thrusts. Bedding orientation and faults indicate ∼N–S shortening. Stations 13827E-H sampled bedding along the ∼NNW-dipping limb of the main Basin anticline: shortening is ∼N–S and the fold axis plunges ∼W (Figure 7c).

The Oligocene-Neogene strata of the Karakul Basin (Figure 2b; Leonov, 2005) form an open-tight syncline with a 50–60°-∼N-dipping, locally overturned southern limb and a flatter northern limb. This syncline is in fault contact with 35–70° ∼S-dipping Cretaceous strata; the fault dips south. Its apparent normal fault geometry may have resulted from folding. The Gissar Batholith gneisses along the southern margin show a vertical scaly foliation, which may be Cenozoic. Stations 1897A-C give bedding and foliation data across the Basin; shortening is ∼N–S (Figure 7d).

4.5. Southern Domain: Poshma-Kuna, Hakimi, Surkh-Shashma, Guliob, Khodzhi-Obi-Garm Basins

In contrast to the Northern and Central Domains, the Southern Domain is dominated by top-to-∼S reverse faults (Figures 8a and 9a). The less common top-to-∼N faults have minor offset. Several ∼E, ∼WNW, and ∼NE-striking faults within the Gissar Batholith are sub-parallel to rivers and may be Cenozoic in addition to those bounding Mesozoic-Cenozoic remnants. This is consistent with the young AFT ages in the Batholith that hint to unmapped Cenozoic faults (Trilsch, Reuter, et al., 2025). The map and Section SD-01 of Figures 8a and 8b characterize that part of the Southern Domain in which the typical ∼E-trend of the structures of the southwestern Tian Shan changes to ∼NE, typical for the Uzbek Gissar to the southwest. Section SD-01 crosses the Poshma-

Figure 7. (a) Geologic map of the Ziddy Basin at the divide between the Central and Southern Domains. (b) Cross sections (traces in panel (a)). Line-length restoration was performed for the N_2 (Section ZD-01), at the top of the Pg_2 (Section ZD-02), and the Cr_2–Cm–T (Sections ZD-03 and ZD-04) horizons. (c) Left: oblique view of a ∼100 m-scale, ∼N-vergent anticline in Oligocene-Miocene strata occupying a triangle structure. Center: structures related to the Gissar Fault at the southern basin margin (13828A, B). Right: bedding along the ∼NNW-dipping limb of the main Basin anticline (13827E-H). (d) Structure of the syncline in the Karakul Basin (stations 1897A-C). Abbreviations see Figures 3 and 4.

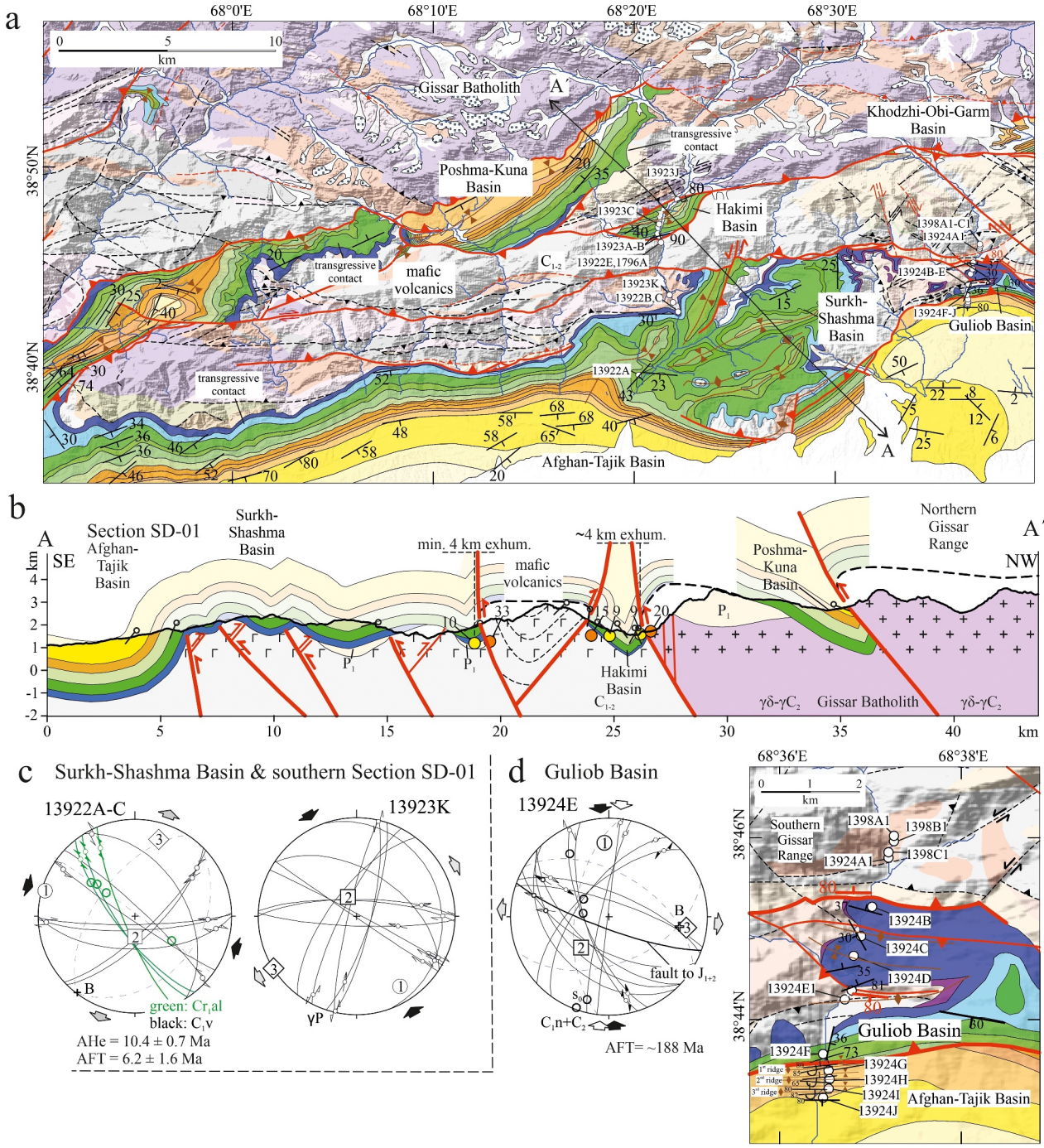

Figure 8. (a) Geologic map of the Poshma-Kuna, Hakimi, Surkh-Shashma, and Guliob Basins of the Southern Domain. (b) Section across most of the basins (trace in panel (a)). (c) Structures of the Surkh-Shashma Basin, highlighting the ~E-striking reverse faults with a dextral and the ~NE-striking reverse faults with a sinistral strike-slip component. (d) Geologic map and structures characterizing the faults in the Guliob Basin and at the contact to the Afghan-Tajik Basin. (e) Sketch highlighting that the ~E-striking faults are reactivated Paleozoic ones and the ~NE-striking ones are newly formed, all formed under ~NW-SE shortening. (f) Map, outcrop images, and structures of the Hakimi Basin. The images characterize anticline-syncline pairs (left) and the northern Basin boundary fault (right). The stereoplots illustrate the top-to-~NE southern Basin-bounding fault (13922E & 1796A), and fault and bedding orientations in the Jurassic-Cretaceous basin strata (13923A, 13923B-C, J, 13922F, 13923A-J). Abbreviations see Figures 3 and 4.

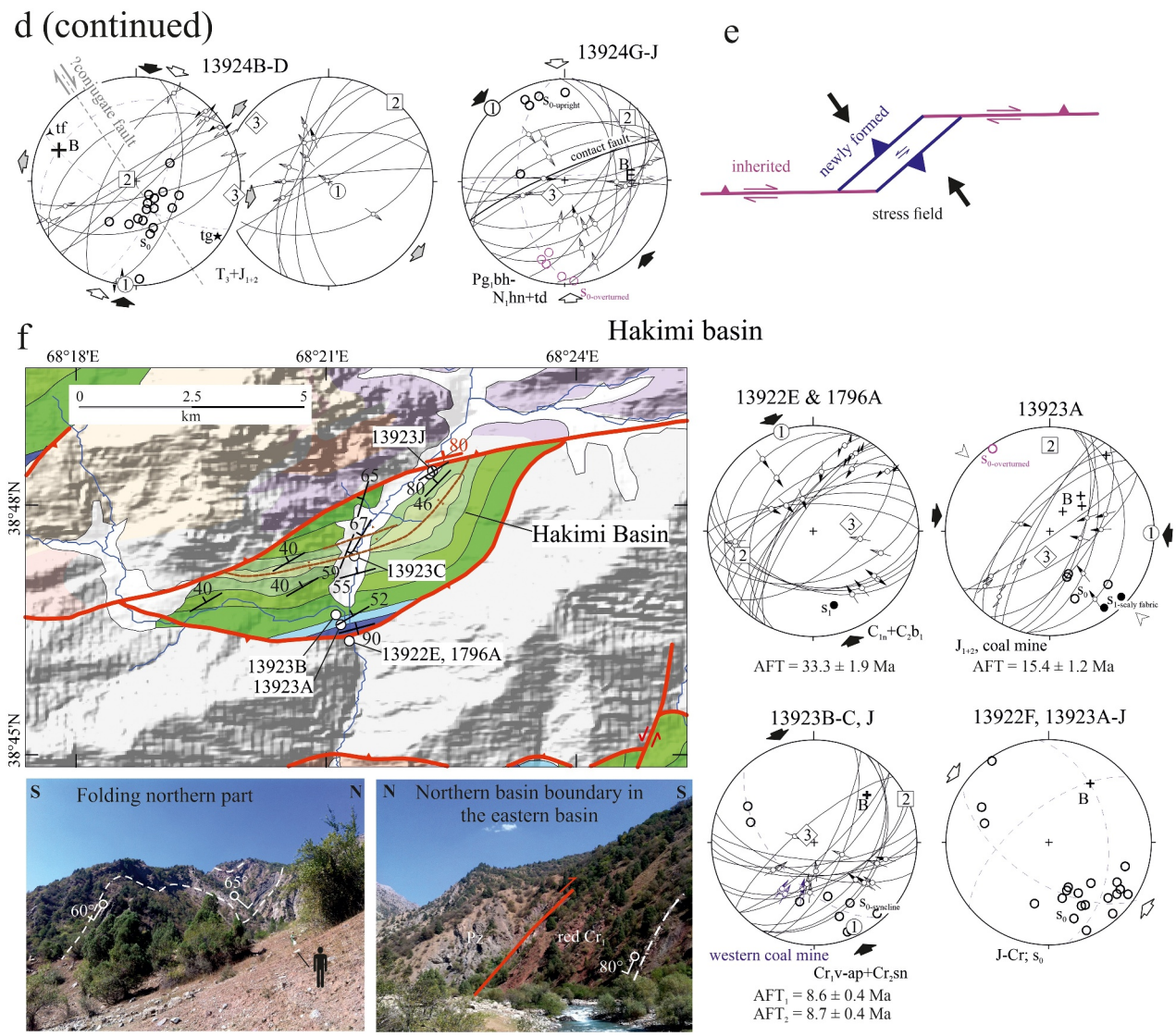

Figure 8. (Continued)

Kuna, Hakimi, and Surkh-Shashma Basins. In comparison with the Khodzhi-Obi-Garm Basin farther east (Figure 9a), it highlights along-strike shortening variations with higher amounts in the west. Top-to-~SSE reverse faults dominate and their vertical offset exceeds that of the ~NNW-vergent faults, for example those that bound the Hakimi and Poshma-Kuna Basins in the SE. As in the Ziddy Basin, the overall dip of their Mesozoic-Cenozoic strata is ~NNE, reflecting the overall ~SE-vergence. Based on the AFT and paleotemperature data, exhumation amounts to ~4 km in the central and northern Hakimi Basin and is less at its southern margin (Trilsch, Reuter, et al., 2025). In Section SD-01, the southern Tian Shan margin is bounded by a top-to-~SE reverse fault that steepens strata in its footwall and has a vertical displacement of ~2 km.

Stations 13922A-C and 13923K (Figures 8a and 8c) sample a traverse with transgressive Surkh-Shashma Basin strata on basement. The structures in the Cretaceous and Paleozoic rocks are similar. Key observations are: (a) The map-scale, ~E-striking reverse faults have a dextral, and the ~NE-striking faults have a sinistral displacement component. (b) Shortening is ~NW–SE and normal to the local fold-axis trends in the Basin. The stations in both the Surkh-Shashma and more eastern Guliob Basins north of the leading fault to the Afghan-Tajik Basin

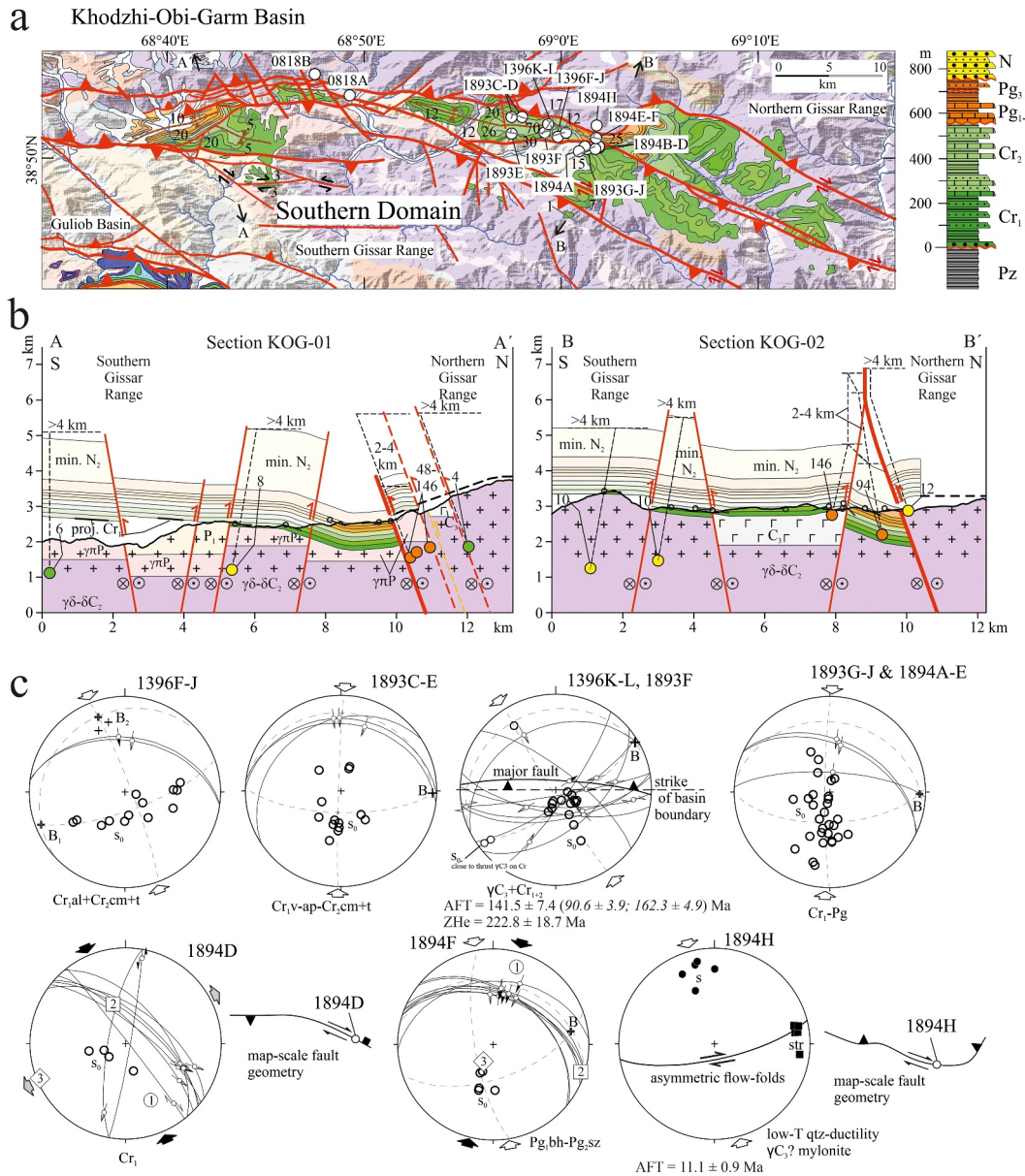

Figure 9. (a) Geologic map of the Khodzhi-Obi-Garm Basin in the center of the Southern Domain. (b) Sections across the western (KOG-01) and eastern Basin (KOG-02); note the difference in vertical displacement between the top-to-~S basin-bounding reverse faults (several km) and the top-to-~N faults (few hundred meters). Line-length restoration was performed for the basement-cover boundary. (c) Structures in the eastern Basin, see text for details. Abbreviations see Figures 3 and 4.

emphasize—with the dominance of strike-slip and local normal faults (station 13924D)—fold-axis parallel, that is, along-strike extension. In the Guliob Basin, the structural trend is ~E and shortening is ~N–S (stations 13924A, 13924B-F; Figures 8d and Figure S5). In station 13924E, the subvertical reverse fault that displaces basement onto Jurassic strata has a ~NW-strike and a strong dextral-slip component, thus is one of the first of similar faults that dominate the area of the Khodzhi-Obi-Garm Basin farther east (Figures 8d and 9a). Across the top-to-~S reverse fault to the Afghan-Tajik Basin, shortening changes to ~NW–SE and thrusts prevail (stations 13924G-J). The shortening direction imposes dextral slip on the boundary fault and on the tight-isoclinal folds that characterize its footwall strata (Figure 8d).

Figure 8f details the structures in the Hakimi Basin. Stations 13922E & 1796A are in greenschist just south of the top-to-~NE reverse fault that bounds the Basin in the south. Diffusion-precipitation creep deformation produced

an anastomosing scaly s-c fabric with calcite veins and calcite on foliation and shear planes; shortening is—as in the entire Hakimi Basin—~NW–SE. Just to the north, a coal mine exploited thickened Jurassic strata that form a ~100 m-wide syncline with a vertical southern limb. The southward thickening, steepening, and local overturning of the strata toward the bounding fault indicates a trishear geometry. Stations 13923A-C, J and 13922F collect fault and bedding orientations over most of the Basin: shortening is ~NW–SE and the Basin-internal tight folds plunge ~NE; the considerable orientation scatter of the structural elements is due to changes in the plunge angle.

Sections KOG-01 and KOG-02 (Figures 9a and 9b) across the Khodzhi-Obi-Garm Basin show that all top-to-~N faults, except the northernmost one in Section KOG-02, have vertical offsets of <200 m. The offsets along the top-to-~S faults that bound the Basin in the north are higher—>2 km—as indicated by the change from partial-reset to reset AFT ages. Strata dip 25–30°—locally 70° north—along the northern Basin margin but are sub-horizontal with morphologically distinct flat surfaces in most other parts (Figures 9a and 9b; Käßner et al., 2016); consequently, shortening is low. Käßner et al. (2016) showed that the northern border of the western Khodzhi-Obi-Garm Basin is a top-to-~S reverse fault with a dextral strike-slip component (their stations 0818A & B). Our stations cover the eastern Basin where the main fold-axis trend is ~ENE (Figures 9a and 9c). At stations 1396F-J, we mapped ~NNE-trending folds that interfere with the former. In connection with the documented dextral transpression (see below), we relate this pattern to the strike-slip component. Stations 1893C-E document the open syncline of the northern part of Section KOG-02. Stations 1396K-L and 1893F cross the northern Basin boundary: only locally, the Cretaceous strata are overturned in the reverse-fault footwall and the fault has a strong dextral-slip component. Stations 1893G-J and 1894A-E comprise a short traverse crossing a fold and a major fault: the fold is tight (~E-trending axis) with a few thrusts, shortening is ~N–S, and thrusting top-to-~S with gliding in bedding. Station 1894D characterizes the major fault, which is characteristic for the many ~WNW-striking faults in the eastern Khodzhi-Obi-Garm Basin. It separates locally exposed basement and Cretaceous-Paleogene strata and has 100–200 m dextral offset; the measured faults are Riedel shears to the map-scale fault and have dextral, weakly transtensional kinematics; bedding is rotated clockwise into a ~NE dip. Station 1894F is off the main fault in Paleogene shale and oyster beds, shows pre-folding and syn-folding (gliding in bedding) faults with ~NNE–SSW shortening, and has no strike-slip component. Deformation is thus partitioned between strike-slip along discrete faults and regional shortening by folding and thrusting. Station 1894H samples a low-temperature granitoid mylonite with quartz-ductility in the fault zone that places basement against Paleogene rocks at the northern Basin rim: asymmetric folds indicate dextral shear along the vertical shear zone and deformation is Cenozoic based on a ~11 Ma AFT age (Trilsch, Reuter, et al., 2025).

In the Southern Domain, the ~E-striking faults follow the structural trend of the Paleozoic basement of the western Tian Shan and have a significant dextral strike-slip component; they are inherited (Figure 8e). The ~NE-strike of many of the Cenozoic structures is abnormal for most parts of the southwestern Tian Shan and follows that of the Uzbek Gissar farther southwest (Figure 2a). These ~NE-striking faults cut the lithologic and structural grain of the basement and are thus newly formed. The folded Mesozoic-Cenozoic strata are detached, involving basement. The faults in the meta-volcanic and -sedimentary basement rocks of the Uzbek Gissar that are certainly Paleozoic (as sealed by Mesozoic-Cenozoic strata) also have a ~E-strike, implying that the dominant ~NE-striking faults there are newly formed Cenozoic ones (Figure 8e).

4.6. Along-Strike Extensions: Intra-Montane Basins of the Seven Lakes, Garm Massif, and Alai Range

Figure 10 interprets the Cenozoic structures along the Seven Lakes valley south of the Khstut-Zavron Basin in the Central Domain. The Seven Lakes are dammed by rockfall deposits, which together with other lakes in the southwestern Tian Shan are interpreted as mostly earthquake-induced (e.g., Barbosa et al., 2021; Havenith et al., 2015). Mapping of the neotectonic faults is hindered by the rugged terrane and the widespread massive limestone lithology. Besides the Malguzar and Magyan Basins, which can be traced over 10s-of-km along strike, we mapped three new tectonic slices of Jurassic rocks, tracing Cenozoic faults. Most basin relicts are fault-bounded in the south and transgressive in the north. The stations (Figure 10) show ~N–S shortening from the folded bedding, and ~NW–SE shortening from the meso-scale faults, indicating deformation partitioning with folding in the basins and dextral transpression along the border faults. Stations 1899A and B stand out, as their major-displacement faults are both polished and covered with cm- to dm-long calcite fibers, and are accompanied by a sub-vertical, scaly rock fabric. We interpret the calcite fibers as indicating creep after seismic slip.

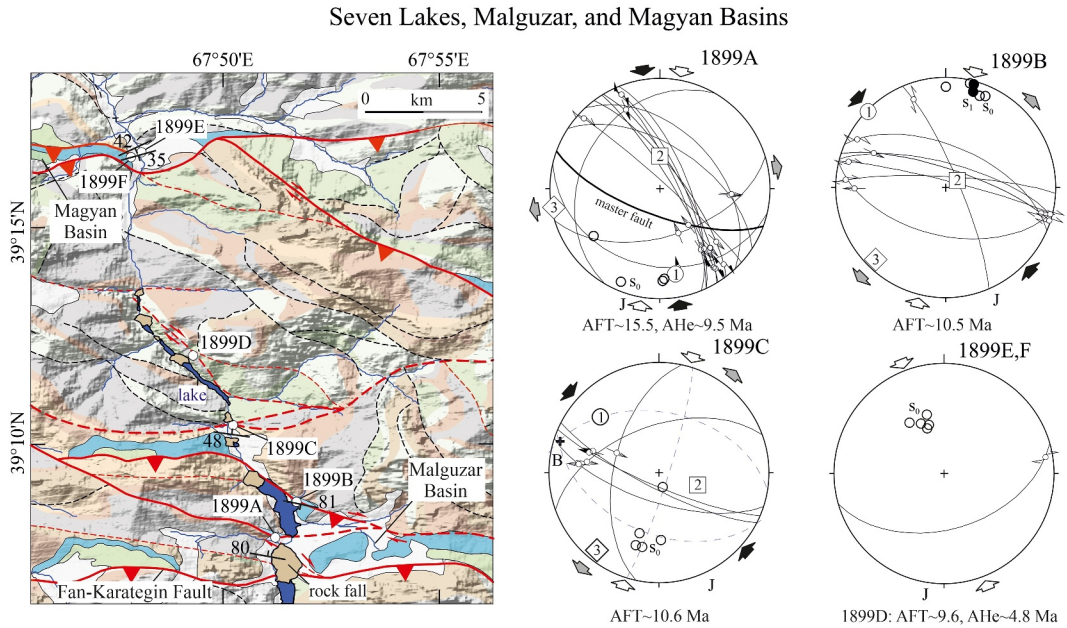

Figure 10. Geologic map of the Malguzar and Magyan Basins and several, partly newly mapped, Jurassic tectonic slices along the Seven Lakes valley. Blue and brown polygons outline the lakes and the rockfall deposits that dammed them. Black dashed lines are Paleozoic faults. The stereoplots highlight the folding with ~N–S shortening in the Jurassic strata and the major dextral strike-slip component along the reverse faults that bound them. Abbreviations see Figures 3 and 4.

Table 1
Line-Length Shortening for Individual Horizons and Cross Sections

Section	Horizon (top)	Shortening (km)	Shortening (%)
SL-01	Pg_{1-2}	0.8	11
KZ-01	Cr_2–Cm–T	0.7	5
Z-01	Cr_2–Cm–T	2.3	20
Z-02	Pg_{1-2}	1.1	18
Z-03	Cr_2–Cm–T	1.5	18
Z-04	Cr_2–Cm–T	2.5	31
FY-01	J	1.7	18
FY-02	J	1.2	15
FY-03	J	2.2	28
ZD-02	Pg_2	1.3	28
ZD-03	Cr_2–Cm–T	0.8	10
ZD-04	Cr_2–Cm–T	0.5	8
KOG-01	Basement	0.1	1
KOG-02	Basement	0.1	1
SD-01-PK	Cr_1	1.3	14
SD-01-HK	J	2.2	29
SD-01-SS	Lower Cr_1	2.7	12

Note. PK = Poshma-Kuna Basin; HK = Hakimi Basin; SS = Surkh-Shashma Basin. Pg_{1-2} = Paleocene-Eocene, Cr_1 = Lower Cretaceous, Cr_2–Cm–T = Upper Cretaceous–Cenomanian–Turonian, J = Jurassic.

Figure S6a interprets the Cenozoic structures of the Garm Massif to the east of our main study area with the intention to correlate major faults over >100 km along strike. The Zeravshan and the Fan-Yagnob Fault systems bound the Karategin Basin north of the Garm Massif; the Karakul-Ziddy Fault system with the Anzob and Gissar Faults border the narrow Obi-Safia Basin system along the northern margin of the Garm Massif. Local features, interpreted by a significant dextral strike-slip deformation component, are: (a) A series of ~NNW-striking normal faults that bound folded basin strata between the Anzob and Gissar Faults (① in Figure S6a), and (b) transpressive strike-slip duplexes (②, ③). Stations 17915B, D, and F all record dextral transpressive kinematics along the Anzob Fault zone (Figure S6b).

Stations 1498A-C typify structures of a key outcrop in the southernmost Tian Shan west of the Alai Basin (Figure 2a for location, Figure S7). Within 50–100 m of the leading edge of the Pamir Frontal Thrust—here salt-rooted and mostly concealed by landslides—bedding in Devonian basement limestones dips 30–70° (mostly 60°) southeast. The bedding is in part reactivated by cataclastic faults with striae that plunge more shallowly than the bedding dip-direction and record a dextral component on the faults. Non-reactivated faults are either dextral-oblique reverse or ~E-striking dextral strike-slip faults. Due to the closeness to the Pamir Frontal Thrust and the cataclastic nature of the faults—unusual for Paleozoic fabrics—we interpret the faulting as Cenozoic. The fault zone outlined by these stations must root in a detachment below the Pamir Frontal Thrust that propagated into the Tian Shan basement.

The Alai Range north of the Alai Valley of the eastern southwestern Tian Shan (Figure 2a) hosts several intra-montane basins that were studied for structural geometry, paleostress, and seismotectonics (Coutand et al., 2002; Kufner, Schurr, Ratschbacher, et al., 2018; Przhiyalgovskii &

Lavrushina, 2020; Sippl et al., 2014). Figure S8 extends the map of Sippl et al. (2014) westward, interprets the map regarding Cenozoic structures, and plots structural data from key stations. The Mesozoic-Cenozoic remnants of the NW-Alai Valley are in part transgressive on the basement (low-relief erosional surface), dip ~SW, and are covered by sub-horizontal Pliocene and Quaternary strata. Stations TS19-TS22 (Figure S8) record ~NNW–SSE shortening by thrusting and conjugate strike-slip faulting in both the hanging walls and footwalls of reverse faults; the major ~E-striking structures have a weak dextral strike-slip deformation component. The Kichi-Karakol Basin and its surrounding basement show the following features: (a) The structural trend changes from ~E (NE) to ~NNE, a feature possibly inherited from the Paleozoic orogen (e.g., Burtman, 1975). Thus, the Cenozoic faults appear inherited, with the likely exception of the dextral-transpressive fault zone characterized by stations TS1 and TS16 (Figure S8), which has an ~E-strike and cuts Paleozoic structures. (b) In most of its southwestern part, the Kichi-Karakol Basin forms a monocline, changing dip from 45–55° in the northwest to 30–40° in the southeast; locally, a narrow syncline crops out in the SE with a steep southeastern limb (station P77; Figure S8). Additional folds appear in the stronger shortened NE part of the Basin. (c) The southeastern border is a top-to-~NW reverse fault with a sinistral strike-slip component (stations TS4, P78; Figure S8) and is accompanied by conjugate top-to-~SE meso-scale thrusts that either cut bedding (station TS5) or reactive it (station TS10). The major reverse fault shows a splay with sinistral-transtensive kinematics (station P78) cutting off a basement slice; transgressive Pliocene (N_2) strata (station P78; Figure 6 of Przhiyalgovskii & Lavrushina, 2020) on this slice indicate that a major proportion of Cenozoic shortening/exhumation was pre-Pliocene, similar to the observation south of the Khstut-Zavron Basin. (d) At the southwestern Basin tip, where basement thrusted over Cretaceous strata (stations TS2-TS4), limestones show low-temperature ductility. The calcite lattice preferred orientation indicates that twinning and the rhomb-glide in (11–20) (<a>) were important mechanisms (e.g., Pieri et al., 2001), and deformation occurred under dominant co-axial conditions (texture asymmetry diagram, lower right, Figure S8; Ratschbacher, et al., 1991).

5. Discussion

5.1. Intra-Montane Basin Deformation: From Individual Basins to a Regional Deformation Field

Here, we return to the questions: (a) What is the structural style of deformation? (b) How is strain distributed? (c) Is strike-slip shear playing a role in the overall convergence? (d) How do the current rate and distribution of deformation—measured by GNSS and seismicity—compare to those active over geologic time scales? The answers to these questions should result in the definition of a regional deformation field for the southwestern Tian Shan and allow a comparison with that of the adjacent Afghan-Tajik Basin FTB and the Pamir.

5.1.1. Structural Models and Shortening Estimates

Due to the low-resolution of mapping (1:200.000) and traverse style structural surveys (our study; Käßner et al., 2016; Leonov, 2005; Rogozhin, 2004) and—in particular—the lack of seismic and borehole data, a thorough discussion on fold-fault models that best describe the intra-montane basin structure of the southwestern Tian Shan is premature. Where exposed and accessible, we observed faulted fault-propagation folds with rounded footwall synclines, departing from the classic kink-band geometry. Although hard to depict on the scale of our cross sections, we commonly observed changes in bed thickness in the footwall synclines, also showcased by the widespread occurrence of Jurassic coal in the syncline cores. These thickened synclines are bounded by a single basement-cored fault. Along and away from the axial planes, the footwall synclines show up-section thickness and tightness changes. These geometries are best described by trishear models (Allmendinger, 1998; Erslev, 1991), with the trishear zone exposed at various structural levels and with variable propagation to slip ratios.

Table 1 provides the shortening estimates along the Sections across the individual basins; they range from 1% to 31%. From north to south, the relative shortening values are: Shakristan-Leilyak = 11%, Khstut-Zavron = 5%, Zeravshan = 18%–31%; Fan-Yagnob = 15%–28%; Ziddy = 8%–28%; Khodzhi-Obi-Garm = 1%; Poshma-Kuna = 14%; Hakimi = 29%; Surkh-Shashma = 12%. The high shortening in the Zeravshan Basin could have been facilitated by the thin, often loosely compacted deposits that controlled the fold wavelengths, and the presence of Paleogene evaporites that enabled propagation of thrusts into the basins along shallow detachments. Besides folds and faults, Cenozoic shortening occurred by tilting of the low-relief erosional surface formed prior to Mesozoic-Cenozoic deposition. The surface is best preserved where basin strata transgressed onto basement

rocks and where relict Jurassic-Cretaceous strata occur. Whereas in the Kyrgyz and Kazakh Tian Shan the surface dips ≤10° in most areas (e.g., Abdrakhmatov et al., 2001; Morin et al., 2018; Sobel et al., 2006), its remnants dip up to 40° in the southwestern Tian Shan, for example, north of the Zeravshan and Fan-Yagnob Basins. Sub-horizontal dips occur as well, for example, in the Khodzhi-Obi-Garm Basin.

On the scale of the southwestern Tian Shan, shortening calculated from the basin strata and dip of the low-relief erosional surface is highest in its central part—along the Zeravshan and Fan-Yagnob Basins—and decreases north- and southward, as already concluded by Rogozhin (2004). The N–S shortening variation may partly reflect the rheologic structure of the Paleozoic orogen. The Gissar Batholith granitoids were less amenable to strain concentration than the heterogeneous, bedded, and foliated rocks of the Central and Northern Domains. The low strain is reflected by the weakly deformed strata of the Khodzhi-Obi-Garm Basin atop the Batholith. Trilsch et al.'s (2025) thermochronologic data provide support: they showed that shortening propagated rapidly from the Pamir into the southwestern Tian Shan. The part that lagged behind was the Gissar Batholith; its younger AFT ages suggest that after reactivation of the major Paleozoic faults in the Central and Northern Domains, the Cenozoic faults within the Batholith may have formed when shortening rates in the Central and Northern Domain had decreased.

Adding up the highest shortening values of the sections across the studied basins—from the Shakristan-Leilyak Basin in the north to the Surkh-Shashma Basin in the south—yields ∼7 km total shortening, certainly a minimum. Restoring a regional cross section (Figure S10; Text S1 in Supporting Information S1 for construction details) with undeformed, untilted basement blocks between the major faults yielded ∼15 km total shortening. To estimate the maximum shortening, we extrapolated the maximum shortening determined in the basins (Sections KOG-02, ZD-02, FY-03, Z-03, and SL-01) to the adjacent basement blocks; this yielded ∼40 km. The GNSS-derived shortening rates for the area in Figure 2b (∼3 mm/yr; range 1.3–6.2 mm/yr, mean = 3.36 mm/yr, median = 2.67 mm/yr, $n = 9$; data compiled in Metzger et al., 2021) would imply ∼40 km shortening, if extrapolated to ∼13 Ma, the preferred age for the onset of major mountain building (Trilsch, Reuter, et al., 2025). Long-term extrapolation is likely justified, as a majority of temperature-time models indicates continuous cooling since 15–10 Ma for the southwestern Tian Shan (Trilsch, Reuter, et al., 2025).

If our estimates are regionally significant, the southwestern Tian Shan shows stronger shortening than the eastern Tian Shan. This is supported by the narrower basin widths as well as younger AFT and AHe ages (Trilsch, Reuter, et al., 2025), and higher recent denudation rates in the southwestern than eastern Tian Shan (Kudriavtseva et al., 2023). At least in the central southwestern Tian Shan, the narrowness of the basins and their formation since 15–10 Ma contrast with the broader basins and younger basin deformation in the eastern Tian Shan (<1 Ma, e.g., Jumgal Basin, Coddington & Burgette, 2020; Naryn Basin, Goode et al., 2014). Similar to the Kyrgyz-Kazakh Tian Shan (e.g., Abdrakhmatov et al., 2001; Thompson et al., 2002), few major Cenozoic faults govern the deformation of the southwestern Tian Shan; these are the Nuratau-Kurganak-Rasraut, N- and S-Zeravshan, Fan-Yagnob, Fan-Karategin, Karakul-Ziddy, Gissar-Obi-Garm and the S-vergent thrust along the southern Tian Shan margin (Figure 2).

5.1.2. Regional Deformation

A general observation from our field survey of the southwestern Tian Shan is that although linear in map view, most of the top-to-∼N reverse faults dip ≥50°; the top-to-∼S faults often dip steeper, up to 80°. In most cases, the intermediate to steep dips of the Cenozoic faults follow the Paleozoic basement structure. Together with the position of these faults along distinct basement-block boundaries, this implies that most major Cenozoic faults are reactivated Paleozoic ones. Focusing on the regional fault pattern, we observed tripartite first-order Cenozoic structural trends in the southwestern Tian Shan, including the Uzbek Gissar (Figures 1a and 2). Figure 11a visualizes these trends schematically. In the Northern Domain, Cenozoic faults and folds strike/trend ∼E to ∼ENE, follow the Paleozoic structures, and form a gentle, southward-concave arc that is traced by the Turkestan and Zirabulak Sutures. Along one segment of the Nuratau-Kurganak-Rasraut Thrust Belt, we observed strike-slip accompanying the reverse faulting. Shortening directions calculated from both folded bedding and fault-striae data are ∼N–S and correspond to the orientation of the GNSS vectors in the Northern Domain and the Fergana Basin (Figure 11b). In the Central Domain, the structural trends are more heterogenous, but two dominate: (a) An ∼E-trend that follows the basement grain, with the Cenozoic faults being reactivated Paleozoic ones; (b) a ∼(W)NW-trend, for which we documented a component of dextral shear, for example, in the southeastern corner

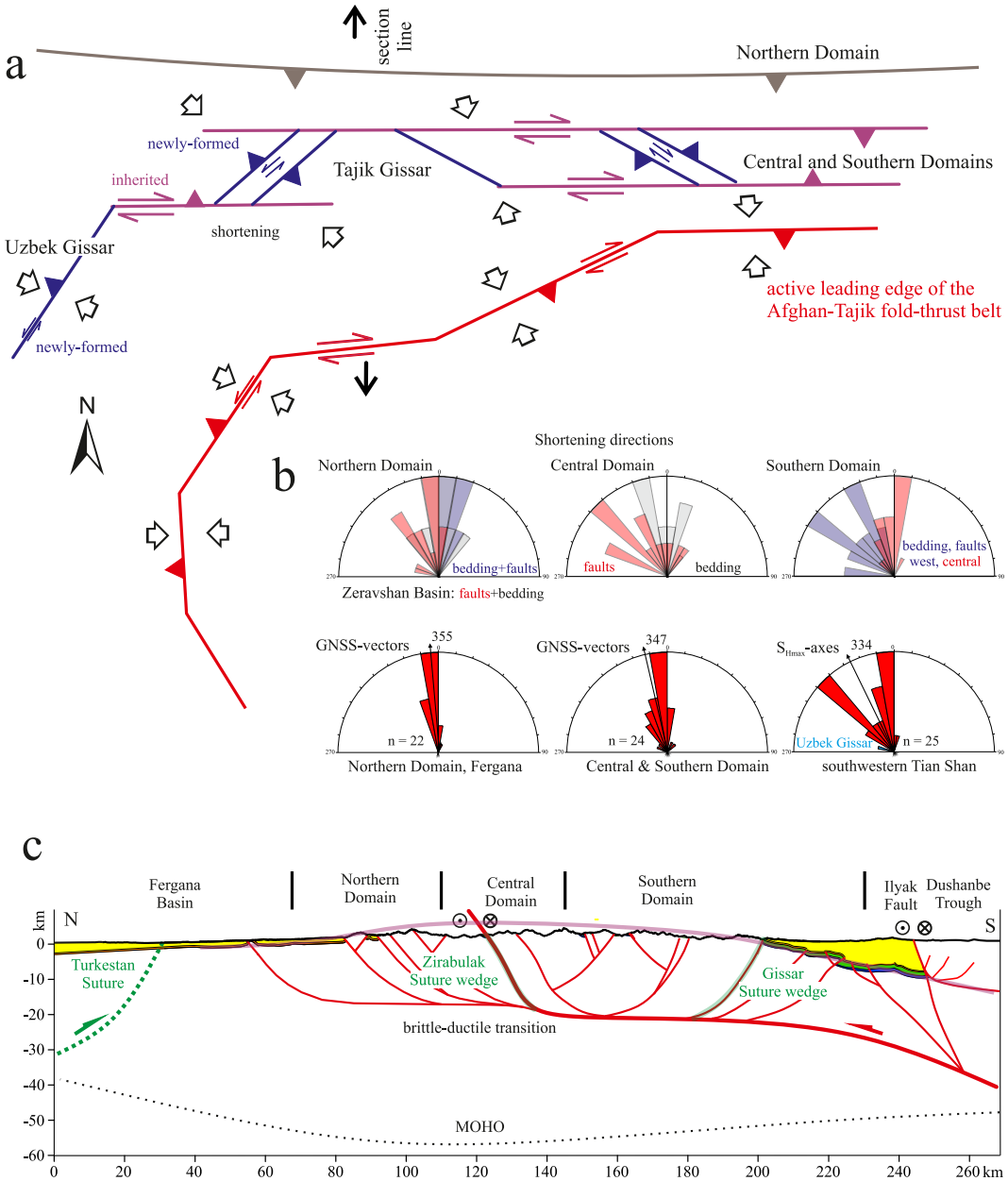

Figure 11. (a) Schematic visualization of the tripartite Cenozoic structural trends in the southwestern Tian Shan, including the Uzbek Gissar, and the kinematics along the related main faults. The Northern Domain structures strike ~E and reactivate the Paleozoic ones. In the Central Domain, the ~E-trend also comprises reactivated Paleozoic structures; the ~(W)NW-striking faults accommodated a component of dextral shear, and at least some of them formed anew and are not reactivated Paleozoic ones. In the Southern Domain and the Uzbek Gissar, the ~E-trend follows the structural grain in the Paleozoic Gissar Batholith and its host rocks. The ~NE-trend, dominant in the Uzbek Gissar and the western Southern Domain, comprises thrusts that formed anew in the Cenozoic; the ~WNW-striking faults have a strong dextral strike-slip component, and are in part newly formed in the Cenozoic. The red line below the sketch of the structural trends and kinematics of the southwestern Tian Shan shows— for comparison—the trends and kinematics of the active leading edge of the Afghan-Tajik Basin fold-thrust belt (data in Gągała et al., 2020; Metzger et al., 2021). (b) Shortening directions determined from folded bedding and fault-striae data visualized in rose diagrams (this study, upper panel) compared with azimuths of GNSS vectors (compilation in Kufner, Schurr, Ratschbacher, et al., 2018) and SH_{max}-axis azimuths from focal mechanism solutions (Figure 1b). Within the southwestern Tian Shan, ~N-S shortening dominates, but is accompanied by a significant dextral strike-slip component. (c) Depth interpretation of the Cenozoic surface structures mapped in this study along a section across the central southwestern Tian Shan (trace in Figure 2b); the fault dips are interpreted to be governed by the Paleozoic structural grain, determined by the Gissar and Zirabulak suture wedges. The Moho structure is from Schneider et al.'s (2019) receiver-function study and approximate. The convex-down Moho bulge is mirrored by a convex-up topographic envelop, outlined by the base of the Mesozoic-Cenozoic strata. The detachment extends south(west)ward and roots in the delamination zone beneath the Pamir (see Figure 12b).

of the Khstut-Zavron Basin, along faults in the Seven Lakes traverse, the eastern Zeravshan Fault, the ∼NW-striking section of the S-Fan-Yagnob Fault in the western Fan-Yagnob Basin, and along the Karakul-Ziddy-Fault at the western termination of the Ziddy Basin. At least along the Seven Lakes transect and in the Fan-Yagnob Basin area, such faults cut the Paleozoic fault, bedding, and foliation strikes, indicating that these are in part newly formed faults. Shortening directions calculated from folded bedding are ∼N–S, those from the fault-striae data are ∼NW–SE, highlighting dextral strike-slip on both the ∼E and (W)NW-striking faults (Figure 11b). The Zeravshan-Basin data, plotted in the diagram of the Northern Domain, also show this pattern, as they record deformation along the near field of the N-Zeravshan Fault. South of the Karakul-Ziddy Fault, in the Southern Domain and the Uzbek Gissar, three trends dominate: (a) An ∼E-trend that dominates the western Khodzhi-Obi-Garm Basin area. It follows the lithologic and structural grain in the Paleozoic Gissar Batholith and its host rocks; (b) a ∼NE-trend, which dominates the Uzbek Gissar, but also the western Southern Domain along the Poshma-Kuna, Hakimi, and parts of the Surkh-Shashma Basin. Shortening in this area also departures from the usual ∼N–S trend and is ∼NW–SE; it is ∼N–S in the central part of the Southern Domain (Figure 11b); (c) a ∼WNW-trend, expressed best in the Khodzhi-Obi-Garm Basin area. These faults have a strong dextral strike-slip, locally even a transtensional component. These trends and associate fault kinematics occur also in the Garm Massif and the western Alai Range. The ∼WNW-striking faults may be in part, the ∼NE striking ones are mostly newly formed in the Cenozoic, as they cut the Paleozoic fabric and the Gissar Suture. Characteristically, the ∼NE-striking basement-rooted thrusts in the Uzbek Gissar dip shallowly, ∼30° (Gągała et al., 2020), typical for newly formed thrusts.

Another striking feature of the intra-montane basins is that they form depressions with inward plunging axes; thus, they are folded overwhelmingly along ∼E-trending axes but also along ∼N-trending axes. This is showcased by the Fan-Yagnob Basin, whose western termination dips up to 70°, the along-strike Section KZ-04 between the Zeravshan and Khstut-Zavron Basins, which traced a basement culmination between two depressions occupied by these basins, and by the faulted fault-propagation fold in the northeastern corner of the Khstut-Zavron Basin (station 18911A; Figure 4f). We interpret the culmination-depression geometry by the action of strike-slip shear that rotated the basin-forming, ∼E-trending fold axes out of their initial sub-horizontal orientation. We also documented that the basin synclines can—in general—be traced along-strike with little orientation variation across the basins. These large-scale folds are cut obliquely by the basin-bounding faults. We suggest that the large folds formed first as cylindrical folds and were in the course of continuing deformation truncated by the faults; fault-displacement variations along strike and the strike-slip component may have imposed the oblique fault-fold interactions.

Figure 11a sketches the outlined structural trends, geometries, and kinematics in the southwestern Tian Shan and compares them to the first-order trends, geometries, and kinematics in the Afghan-Tajik Basin FTB, visualized by its active leading edge. Within the southwestern Tian Shan, ∼N–S shortening dominates but is accompanied by a significant dextral strike-slip component. The GNSS vectors and SH_{max}-axes (Figures 1b and 11b) are in average ∼NNW, supporting a dextral strike-slip component in the neotectonic deformation of the Central and Southern Domains. Shortening directions change anticlockwise from east to west. On first order, the shape of the structural arc outlined by the Central and Southern Domains and the Uzbek Gissar and of the leading edge of the Afghan-Tajik Basin FTB mimic that of the intermediate-depth earthquakes beneath the Pamir (Figure 1a). We derive the following first-order inferences: (a) Extending the conclusion of Käßner et al. (2016), the southwestern Tian Shan is involved in the combined northward motion and westward collapse of the Pamir-Plateau crust. The southern boundary of the Northern Domain, the N-Zeravshan Fault zone with the Khstut-Zavron and Zeravshan Basins, constitutes the northern edge of the crustal area that has accommodated a dextral component; the blue band in Figure 1a outlines this northern edge of the Pamir-Plateau collapse affecting the southwestern Tian Shan. (b) Whereas the Afghan-Tajik Basin FTB is fully detached along its basal evaporite layer (e.g., Bekker, 1996; Bourgeois et al., 1997; Gągała et al., 2020), the reactivation of the Paleozoic basement faults and the formation of new Cenozoic faults in the basement requires a deeper detachment. As the deformation field in the southwestern Tian Shan and the Afghan-Tajik Basin FTB form a kinematic continuum, this detachment must underly the Afghan-Tajik Basin and should root in the lithosphere-scale delamination zone beneath the Pamir (see Section 5.2).

5.2. Deep Structure and Relation to the Pamir

Figure S11 shows the result of a 2D forward model along a section from the Dushanbe Trough of the northern Afghan-Tajik Basin to the southern Fergana Basin. Due to the lack of geophysical constraints, it is too schematic

to provide reliable shortening estimates, but—although speculative—it aids interpreting the sub-surface structure. Construction constraints were: (a) As the low-relief erosional surface is rarely preserved, we took the maximum elevation of mountain ridges and/or the exhumation values from the thermochronologic data (Trilsch, Reuter, et al., 2025) as the vertical distance to the base of the eroded Mesozoic-Cenozoic strata. (b) We used the strata thicknesses compiled in Figure S2 and interpolated between the basins. (c) The geometry and kinematics of the faults at the surface are from the field data. (d) The sub-surface geometries of the faults are unknown. We used listric geometries, as interpreted by W. Li et al. (2022) based on seismic tomography in the Kyrgyz Tian Shan. Both listric and sigmoidal fault geometries are able to explain the observed surface geometries. (e) The relative regular 15–25 km spacing of the basins that defines the minimum basement-block widths and the related wavelengths of regional folds indicate a detachment at 15–25 km depth (Figure S11; e.g., Amos et al., 2007; Seeber & Sorlien, 2000), likely coinciding with the brittle-ductile transition. We separated the forward model into two parts to (a) emphasize the distinct structural vergence in the Central and Northern Domains and the Southern Domain, and (b) highlight the uncertainty of the connection of both systems. The Paleozoic sutures may have influenced the Cenozoic structures: the ∼N-dipping Gissar and the ∼S-dipping Zirabulak Sutures likely put control on the overall vergences in the different Domains by structural inheritance. The Cenozoic detachment at the brittle-ductile transition is likely independent of these sutures.

Now, we return to question (v): How is the deformation in different parts of the Tian Shan related to the Indian mantle-lithosphere indenter? Figure 11c shows an interpretation of the subsurface structure along a ∼N–S cross section in the central part of Figure 2b. No interpretation is given for the structure north of the Northern Domain; it likely is governed by the ∼N-dipping wedge associated with the Turkestan Suture, as indicated by ∼S-vergent structures (Rogozhin, 2004). The Moho structure shown in Figure 11c is from Schneider et al.'s (2019) receiver-function study, and although the southwestern Tian Shan and the Fergana Basin are marginal to their network, likely the most accurate. The general pattern (crustal-thickness isolines) is reproduced by the lower-resolution results derived from gravity (Steffen et al., 2011), elevation, geoid-anomaly, and thermal-analysis (Robert et al., 2017) data. The Fergana and Afghan-Tajik Basins are underlain by 40–50 km-thick and the southwestern Tian Shan by ≤65 km-thick crust; the crust south of the Afghan-Tajik Basin is ∼65 km-thick. Thus, the N–S section of Figure 11c shows a convex-down Moho bulge, mirrored by a convex-up topographic envelop, outlined by the base of the Mesozoic-Cenozoic strata, which—on first order—corresponds to the low-relief erosional surface (magenta arc in Figure 11c). Figure 12a traces the Moho culminations (yellow, under the basins) and depressions (green, under the ranges). The Moho of the Afghan-Tajik Basin dips steeply SE. This is a result of the indenting Indian mantle lithosphere leading to delamination of the Basin's lithosphere (Schneider et al., 2019). The Moho culmination follows the ∼NE-trending trough axis of the Afghan-Tajik Basin and the depression under the southwestern Tian Shan lies within its northern part. Thus, during the progressive indentation and the delamination of Asian lithosphere, the foreland ahead of the indenter must have been loaded and depressed; this foreland comprised the basement of the Afghan-Tajik Basin and the southwestern Tian Shan. As the Basin lithosphere delaminated toward west and north (Kufner et al., 2016), the foreland loading provided space north and west of the Pamir into which the Pamir-Plateau crust found space to collapse; this foreland included the southwestern Tian Shan.

Where does the detachment beneath the southwestern Tian Shan root? Figure 12b combines our section across the Tian Shan (Figure 11c) with section B of Gągała et al. (2020) across the Afghan-Tajik Basin FTB, and its possible connection with the delamination zone beneath the Pamir (modified from Figure 2b of Abdulhameed et al., 2020, and Figure 18c of Gągała et al., 2020). Kufner, Schurr, Ratschbacher, et al. (2018) showed that seismicity below the Ilyak and the Darvaz Faults extends far below the evaporite detachment of the Afghan-Tajik Basin FTB. Thus, we interpret both faults as crustal-scale ones. The detachment beneath the southwestern Tian Shan would deepen southeastward (forming a ramp, ① in Figure 12b), mimicking the south(east)ward deepening of the base of the Mesozoic-Cenozoic strata (Figure 12b, region of the Ilyak Fault). Seismic clusters underneath the highly shortened thrust stacks of the Vakhsh and Kulyab anticlinoria possibly trace other crustal-scale faults, interfering with the evaporate detachment. The sinistral Darvaz Fault would accommodate the faster northward motion of the Pamir-Plateau crust than the major part of the Afghan-Tajik Basin to its northwest. Its recent sinistral-transtensional kinematics (Metzger et al., 2021) indicates that it is currently displaced together with the Pamir-Plateau crust northwestward.

Combining the ∼90 km thin-skinned shortening along section B of Gągała et al. (2020) across the Afghan-Tajik Basin FTB with our estimates for the southwestern Tian Shan yields 105–130 km total shortening in front of the

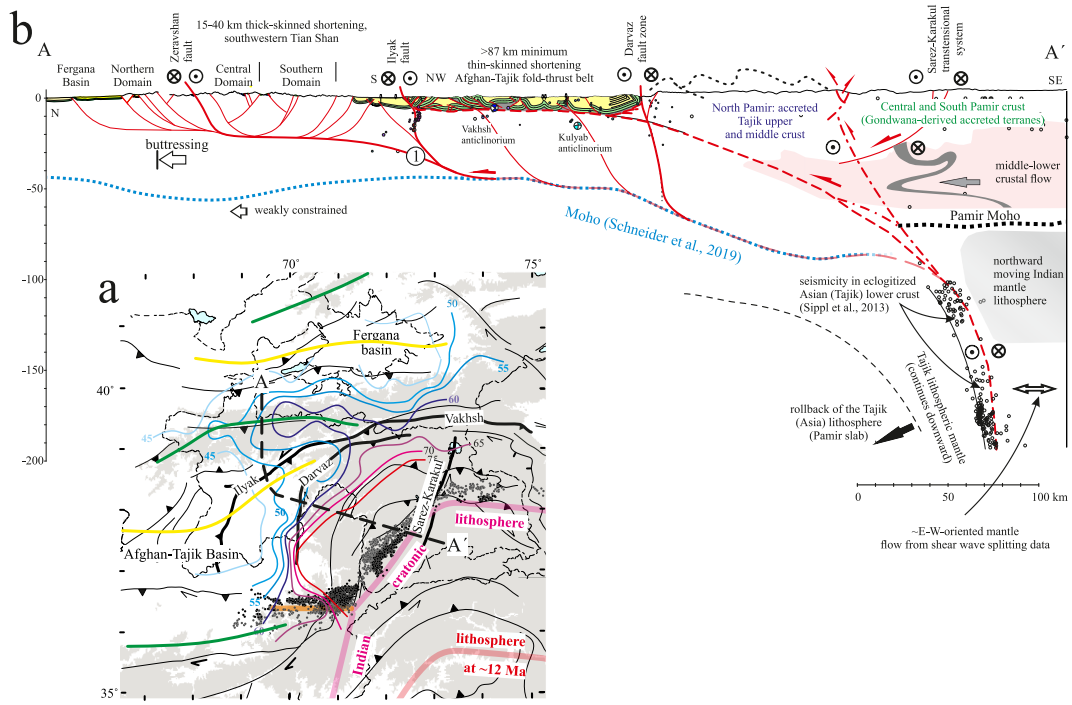

Figure 12. (a) Map of the western tip of the India-Asia collision zone with surface structures (major Cenozoic faults) and Moho contours from the receiver-function study of Schneider et al. (2019) (colored lines with depth in km), and intermediate-depth earthquakes, outlining the Hindu Kush slab (northward subduction of marginal Indian lithosphere) and the Pamir slab, Tajik (Asian) lithosphere delaminating in front of the Indian mantle indenter below the Pamir (from Bloch et al., 2021; Sippl et al., 2013). The yellow and green lines mark Moho culminations and depressions, respectively. (b) Cross-sectional sketch of the crustal-scale structures from the southwestern Tian Shan (this study), across the Afghan-Tajik Basin fold-thrust belt (FTB) (section B of Gągała et al., 2020), into the delamination zone outlined by the slab beneath the Pamir (cf. Abdulhameed et al., 2020; Gągała et al., 2020). The geometries highlight the subhorizontal evaporite-detachment at the base of the Afghan-Tajik Basin FTB, the mid-crustal detachment below the southwestern Tian Shan, and the rooting of several strike-slip (Ilyak and Darvaz faults) and thrust structures of the Afghan-Tajik Basin FTB in the deeper detachment, which is interpreted to run along the Moho. The sinistral-normal Sarez-Karakul fault system and the reddish zone on the right side of the cross section highlight the upper to lower crustal flow from the Pamir-Plateau crust to the foreland. The model geometries and kinematics are akin to models proposed for foreland-directed plateau collapse (Rey et al., 2010). The ~E–W oriented mantle flow below the Indian mantle-lithosphere indenter may contribute to the westward rollback of the Pamir slab.

present northwestern edge of the Pamir (Darvaz Fault) since 15–10 Ma. This is similar to the 100–175 km shortening farther southwest (sections C–E of Gągała et al., 2020) but more than the shortening across the Afghan-Tajik Basin FTB farther northeast along the Pamir thrust front (20–75 km, Gągała et al., 2020; Kley et al., 2023; T. Li et al., 2019). The latter values, however, do not include the shortening in the eastern south-western Tian Shan, which we interpret as driven by shortening above the detachment that roots in the delamination zone beneath the Pamir; still, there will be a mismatch remaining between the ~WNW–ESE shortening across the southwestern Afghan-Tajik Basin FTB and that across the northeastern one. This shortening mismatch corresponds to the different depth extent (slab length) of the delaminating Pamir slab: the intermediate-depth seismicity of its ~N(E)-striking part extends to ≤300 km, the ~E-striking part to ≤200 km (Bloch et al., 2021; Sippl et al., 2013). Although the depth extent of the ~E-striking part, that is tearing and folding (Bloch et al., 2021; Kufner et al., 2016), may be a function of its geometry and thermal structure, its lower length correlates with lower shortening north of it. One solution for this mismatch would be a period of northwestward motion of the Indian mantle indenter (northwestward convergence, e.g., Kley et al., 2023). The India-Asia convergence history does not include a NW–SE-oriented convergence period (e.g., Molnar & Stock, 2009) and σ_1 of the regional stress tensor derived from the intermediate-depth earthquakes aligns with the azimuths of the GNSS vectors in the rigid block of the eastern Pamir and is ~N–S (N13°W; Bloch et al., 2021). Another solution would be westward flow of mantle material below the Indian mantle indenter; this would impose a

westward-directed force on the delaminating Pamir slab. Kufner, Eken, et al. (2018) reported ENE–WSW-oriented fast directions from SKS splitting, which do not conform to the absolute plate motion but do agree approximately with the large-scale ∼E–W trend of SKS-derived fast directions throughout Tibet. They proposed that the northward motion of the Indian plate induces large-scale lateral escape flow in the mantle underneath the Pamir and southwestern Tian Shan.

Seismicity and the GNSS-vector field led to the interpretation that Pamir-Plateau crust is currently moving northward and collapsing westward; if Plateau collapse drives the westward crustal motion, then the Pamir crust needs besides N–S shortening and thickening due to the India-Asia convergence to thin (extend) either homogeneously or by a middle-lower crustal flow zone. Stübner et al. (2013) were first to suggest such a scenario, extended by Abdulhameed et al. (2020): the Shakhdara and Muztagata extensional domes and the Sarez-Karakul rift (Figure 1a) are surface expressions of syn-convergence extension and the partial-molten rocks in the domes may be part of a foreland-directed flow zone that, in our current interpretation, may reach beyond the Plateau (models in Rey et al., 2010) and drive shortening as far as the southwestern Tian Shan. Both the collapse and the flow may be channeled westward by the mayor backstop in the east and northeast: the Tarim-Basin cratonic lithosphere; the Fergana-Basin lithosphere may constitute another, secondary far-field backstop.

6. Conclusions

We aimed to establish the deformation field of the southwestern Tian Shan at the western tip of the India-Asia collision zone. This area faces the Indian mantle-lithosphere indenter beneath the Pamir in its eastern part and is adjoining the area that comprises the westward collapsing Pamir-Plateau crust inverting the Afghan-Tajik Basin and reactivating the Uzbek Gissar, the southwesternmost tip of the southwestern Tian Shan. We define the southwestern Tian Shan as the Tian Shan west of the Talas-Fergana Fault and south of the Fergana Basin.

By analyzing several intra-montane basins, providing maps, cross sections, and structural data collected along ∼N–S traverses, we establish the geometry and kinematics of the main structures and outline the Cenozoic deformation field. In the basins, we observed faulted fault-propagation folds with round footwall synclines, departing from the classic kink-band geometry. Stratigraphic thickness changes in the footwall synclines below the basin-bounding reverse faults, also showcased by Jurassic coal deposits in the syncline cores, and up-section thickness and tightness changes along and away from the axial planes suggest that the fault-fold relationships are best described by a trishear model.

The Nuratau-Kurganak-Rasraut, N- and S-Zeravshan, Fan-Yagnob, Fan-Karategin, Karakul-Ziddy, and Gissar-Obi-Garm Faults and the border fault to the Dushanbe Trough of the Afghan-Tajik Basin dominate the southwestern Tian Shan. The N-Zeravshan and the Karakul-Ziddy Faults follow major units of the Paleozoic orogen and define three Domains (Northern, Central, and Southern). The Cenozoic fault-fold pattern reveals three structural trends. The ∼E-trend follows the lithologic and structural grain of the Paleozoic orogen, that is, the Cenozoic faults reactive Paleozoic ones; the ∼NE-trend dominates the Uzbek Gissar but also the western Southern Domain; the ∼WNW-trend is common in the eastern Southern Domain. The faults of the ∼E- and ∼WNW-trends accommodated dextral strike-slip in addition to dominant ∼N–S shortening; the ∼WNW-striking faults were in part, the ∼NE striking ones were mostly newly formed in the Cenozoic. Most intra-montane basins form depressions with inward plunging axes; thus, they are folded (overwhelmingly) along ∼E-trending axes but also along ∼N-trending axes. We interpret this culmination-depression geometry by the action of strike-slip shear that rotated the basin-forming folds out of their initial sub-horizontal orientation.

The western leading edge of the southwestern Tian Shan, that is, the western Southern Domain and the Uzbek Gissar, shows ∼NW–SE shortening; ∼N–S shortening dominates most of the southwestern Tian Shan, but is accompanied by significant dextral strike-slip. Shortening decreases from the central part of the southwestern Tian Shan toward north and south and from east to west; total Cenozoic N–S shortening amounted to 15–40 km. On first order, the deformation field of the southwestern Tian Shan resembles with its structural trends, geometries, and kinematics that of the Afghan-Tajik Basin FTB to its south, and mimics in shape the geometry of the intermediate-depth earthquake zone beneath the Pamir, which outlines the delamination of the Asian (Tajik-Tarim) lithosphere due to its indentation by the Indian mantle-lithosphere promontory.

The depth interpretation of the Cenozoic surface structures mapped in the southwestern Tian Shan is hindered by the lack of modern geophysical studies. We interpret the fault dips and vergences as governed by the pre-existing

Paleozoic structural grain, that is, determined by the Gissar and Zirabulak suture wedges. The relative regular, 15–25 km spacing of the intra-montane basins defines the minimum basement-block widths and indicates a detachment at 15–25 km depth, likely coinciding with the brittle-ductile transition below the Tian Shan. The Moho structure is only known approximately; likely a convex-down Moho bulge beneath the southwestern Tian Shan is mirrored by a convex-up topographic envelop, outlined by the base of the Mesozoic-Cenozoic strata.

We infer that the southwestern Tian Shan is involved in the combined northward motion and westward collapse of the Pamir-Plateau crust. The southern border of the Northern Domain along the N-Zeravshan Fault zone constitutes the northern edge of this involved crustal area. Whereas the Afghan-Tajik Basin FTB is detached along its basal evaporite layer, the reactivation of the Paleozoic basement faults and the anew formation of Cenozoic faults in the basement requires a deeper detachment underlying both the southwestern Tian Shan and the Afghan-Tajik Basin. As the deformation field in the southwestern Tian Shan, the Afghan-Tajik Basin FTB, and the adjacent Pamir form a kinematic continuum, this detachment should root in the lithosphere-scale delamination zone beneath the Pamir. During progressive indentation and resulting delamination of Asia lithosphere, the foreland ahead of the Indian mantle-lithosphere indenter must have been loaded and depressed; this foreland comprised the basement of the Afghan-Tajik Basin and southwestern Tian Shan. As the Asian lithosphere delaminated toward west and north, the foreland loading provided space north and west of the Pamir into which the Pamir-Plateau crust found space to collapse; this foreland included the southwestern Tian Shan.

We present a schematic crustal-scale cross section that combines our section across the southwestern Tian Shan with a section across the Afghan-Tajik Basin FTB and the delamination zone underneath the Pamir. We argue that the southwestern Tian Shan is part of the deformation field of the Pamir and underlain by a detachment connected to the Pamir lithospheric delamination zone. The geometries of the crustal-scale cross section highlight the sub-horizontal evaporite-detachment at the base of the Afghan-Tajik Basin FTB, the mid-crustal detachment below the southwestern Tian Shan, and the rooting of several strike-slip (Ilyak and Darvaz Faults) and thrusts of the Afghan-Tajik Basin FTB in the deeper detachment, which we interpreted to run along the Moho. The eastern Tian Shan—east of the Talas-Fergana Fault—is different; the detachment rooting in the Pamir delamination zone and underlying the southwestern Tian Shan must end along the eastern margin of the delamination zone, that is, along the western margin of the Tarim craton. Our study also showcases the need for detailed geophysical studies that would shed light on the deep structure of the southwestern Tian Shan.

Data Availability Statement

Supporting Information may be found in the online version of this article. The Supporting Material Tables and Figures, with Figures 1 and 2 provided as shapefiles, are available in Trilsch, Ratschbacher, et al. (2025), GFZ Data Services, https://doi.org/10.5880/fidgeo.2025.001.

Acknowledgments

We acknowledge Sherzod Abdulov, Louis Andreani, Tristan Gause, Solmaz Mohadjer, and Sanaa Reuter for joint fieldwork. Sofia-Katerin Kufner discussed geophysical aspects. Funded by a Graduate and a Thesis-Completion Scholarship from the Saxonian Government (FT), a DAAD travel grant (FT), and DFG-grants Ra442/40 (Project no. 433506869) and 42 (Project no. 520947397) (LR and FT). Open access funding enabled and organized by Project DEAL. We express our gratitude to Petroleum Experts (UK) for providing an academic license of MOVE™. Editor Djordje Grujic, Associate Editor Laura Giambiagi, reviewer Rodrigo Quiroga, and an anonymous reviewer improved the manuscript. Open Access funding enabled and organized by Projekt DEAL.

References

Abdrakhmatov, K., Weldon, R., Thompson, S., Burbank, D., Rubin, C., & Molnar, P. (2001). Onset, style and current rate of shortening in the central Tien Shan, Kyrgyz Republic. *Russian Geology and Geophysics*, *42*(10), 1585–1609. https://doi.org/10.1038/384450a0

Abdulhameed, S., Ratschbacher, L., Jonckheere, R., Gągała, Ł., Enkelmann, E., Käßner, A., et al. (2020). Tajik Basin and southwestern Tian Shan, northwestern India-Asia Collision Zone: 2. Timing of basin inversion, Tian Shan mountain building, and relation to Pamir-Plateau advance and deep India-Asia indentation. *Tectonics*, *39*(5). https://doi.org/10.1029/2019TC005873

Allmendinger, R. W. (1998). Inverse and forward numerical modeling of trishear fault-propagation folds. *Tectonics*, *17*(4), 640–656. https://doi.org/10.1029/98TC01907

Amos, C. B., Burbank, D. W., Nobes, D. C., & Read, S. A. L. (2007). Geomorphic constraints on listric thrust faulting: Implications for active deformation in the Mackenzie Basin, South Island, New Zealand. *Journal of Geophysical Research*, *112*(3). https://doi.org/10.1029/2006JB004291

Avouac, J. P., Tapponnier, P., Bai, M., You, H., & Wang, G. (1993). Active thrusting and folding along the northern Tien Shan and late Cenozoic rotation of the Tarim relative to Dzungaria and Kazakhstan. *Journal of Geophysical Research*, *98*(B4), 6755–6804. https://doi.org/10.1029/92JB01963

Bande, A., Sobel, E. R., Mikolaichuk, A., & Acosta, V. T. (2017). Talas-Fergana Fault Cenozoic timing of deformation and its relation to Pamir indentation. *Geological Society, London, Special Publications*, *427*(1), 295–311. https://doi.org/10.1144/SP427.1

Bande, A., Sobel, E. R., Mikolaichuk, A., Schmidt, A., & Stockli, D. F. (2017). Exhumation history of the western Kyrgyz Tien Shan: Implications for intramontane basin formation. *Tectonics*, *36*(1), 163–180. https://doi.org/10.1002/2016TC004284

Barbosa, N., Andreani, L., Gloaguen, R., & Ratschbacher, L. (2021). Window-based morphometric indices as predictive variables for landslide susceptibility models. *Remote Sensing*, *13*(3), 451. https://doi.org/10.3390/rs13030451

Bazhenov, M. L., Burtman, V. S., & Dvorova, A. V. (1999). Permian paleomagnetism of the Tien Shan fold belt, Central Asia: Post-collisional rotations and deformation. *Tectonophysics*, *312*(2–4), 303–329. https://doi.org/10.1016/S0040-1951(99)00181-X

Bekker, Y. A. (1996). Tectonics of the Afghan-Tajik basin. *Geotektonika*, *1*, 76–82. (in Russian).

Biske, Y. S., Ershova, V. B., Konopelko, D. L., Stockli, D., Mamadjanov, Y. M., & Wang, X. S. (2021). Detrital-zircon geochronology and provenance of Ediacaran–Silurian rocks of the central to northern Tajikistan traverse: Geodynamic implications for the evolution of the Tian Shan. *Gondwana Research*, *99*, 247–268. https://doi.org/10.1016/j.gr.2021.07.013

Bloch, W., Metzger, S., Schurr, B., Yuan, X., Ratschbacher, L., Reuter, S., et al. (2023). The 2015-2017 Pamir earthquake sequence: Foreshocks, main shocks and aftershocks, seismotectonics, fault interaction and fluid processes. *Geophysical Journal International*, *233*(1), 641–662. https://doi.org/10.1093/gji/ggac473

Bloch, W., Schurr, B., Yuan, X., Ratschbacher, L., Reuter, S., Kufner, S.-K., et al. (2021). Structure and stress field of the lithosphere between Pamir and Tarim. *Geophysical Research Letters*, *48*(22). https://doi.org/10.1029/2021GL095413

Bosboom, R., Mandic, O., Dupont-Nivet, G., Proust, J. N., Ormukov, C., & Aminov, J. (2017). Late Eocene palaeogeography of the Proto-Paratethys Sea in Central Asia (NW China, southern Kyrgyzstan and SW Tajikistan). *Geological Society, London, Special Publications*, *427*(1), 565–588. https://doi.org/10.1144/SP427.11

Bourgeois, O., Cobbold, P. R., Rouby, D., Thomas, J. C., & Shein, V. (1997). Least squares restoration of Tertiary thrust sheets in map view, Tajik depression, Central Asia. *Journal of Geophysical Research*, *102*(12), 27553–27573. https://doi.org/10.1029/97jb02477

Brookfield, M. E. (2000). Geological development and Phanerozoic crustal accretion in the western segment of the southern Tien Shan (Kyrgyzstan, Uzbekistan and Tajikistan). *Tectonophysics*, *328*(1–2), 1–14. https://doi.org/10.1016/S0040-1951(00)00175-X

Brookfield, M. E., & Hashmat, A. (2001). The geology and petroleum potential of the North Afghan platform and adjacent areas (northern Afghanistan, with parts of southern Turkmenistan, Uzbekistan and Tajikistan). *Earth-Science Reviews*, *55*(1–2), 41–71. https://doi.org/10.1016/S0012-8252(01)00036-8

Brunet, M.-F., Ershov, A. V., Korotaev, M. V., Melikhov, V. N., Barrier, E., Mordvintsev, D. O., & Sidorova, I. P. (2017). Late Palaeozoic and Mesozoic evolution of the Amu Darya Basin (Turkmenistan, Uzbekistan). *Geological Society, London, Special Publications*, *427*(1), 89–144. https://doi.org/10.1144/SP427.18

Burtman, V. S. (1975). Structural geology of Variscan Tien Shan, USSR. *American Journal of Science*, *275*(A), 157–186.

Burtman, V. S. (2000). Cenozoic crustal shortening between the Pamir and Tien Shan and a reconstruction of the Pamir-Tien Shan transition zone for the Cretaceous and Palaeogene. *Tectonophysics*, *319*(2), 69–92. https://doi.org/10.1016/S0040-1951(00)00022-6

Burtman, V. S. (2008). Nappes of the southern Tien Shan. *Russian Journal of Earth Sciences*, *10*(1), 1–35. https://doi.org/10.2205/2007ES000223

Burtman, V. S. (2010). Tien Shan, Pamir, and Tibet: History and geodynamics of Phanerozoic oceanic basins. *Geotectonics*, *44*(5), 388–404. https://doi.org/10.1134/S001685211005002X

Burtman, V. S., & Molnar, P. (1993). Geological and geophysical evidence for deep subduction of continental crust beneath the Pamir. In *GSA special papers* (Vol. 281, pp. 1–76). Geological Society of America. https://doi.org/10.1130/SPE281-p1

Carrapa, B., DeCelles, P. G., Wang, X., Clementz, M. T., Mancin, N., Stoica, M., et al. (2015). Tectono-climatic implications of Eocene Paratethys regression in the Tajik basin of central Asia. *Earth and Planetary Science Letters*, *424*, 168–178. https://doi.org/10.1016/j.epsl.2015.05.034

Chedia, O. K. (1972). *Southern Central Asia in the recent era of mountain building*. Frunze. (in Russian).

Clarke, J. W. (1984). *Geology and possible uranium deposits of the Fergana region of Soviet Central Asia*. United States Department of the Interior Geological Survey.

Coddington, J. A., & Burgette, R. J. (2020). Fold kinematics and fault slip rates from progressively deformed terraces: Implications for structural evolution of basins in the Kyrgyz Tien Shan. *Tectonics*, *39*(8). https://doi.org/10.1029/2019TC005776

Coutand, I., Strecker, M. R., Arrowsmith, J. R., Hilley, G., Thiede, R. C., Korjenkov, A., & Omuraliev, M. (2002). Late Cenozoic tectonic development of the intramontane Alai Valley, (Pamir-Tien Shan region, central Asia): An example of intracontinental deformation due to the Indo-Eurasia collision. *Tectonics*, *21*(6), 3-1-3–19. https://doi.org/10.1029/2002TC001358

Cui, Q., Huangfu, P., Li, Z. H., Zhao, J., Pei, X., & Shi, Y. (2024). Tarim rotation mechanism and the differential deformation responses along the Tian Shan. *Geophysical Journal International*, *236*(3), 1275–1287. https://doi.org/10.1093/gji/ggad480

Dedow, R., Franz, M., Szulc, A., Schneider, J. W., Brückner, J., Ratschbacher, L., et al. (2020). Tajik basin and southwestern Tian Shan, northwestern India-Asia collision zone: 3. Preorogenic to synorogenic retro-foreland basin evolution in the eastern Tajik depression and linkage to the Pamir hinterland. *Tectonics*, *39*(5). https://doi.org/10.1029/2019TC005874

De Grave, J., Glorie, S., Buslov, M. M., Izmer, A., Fournier-Carrie, A., Batalev, V. Y., et al. (2011). The thermo-tectonic history of the Song-Kul plateau, Kyrgyz Tien Shan: Constraints by apatite and titanite thermochronometry and zircon U/Pb dating. *Gondwana Research*, *20*(4), 745–763. https://doi.org/10.1016/j.gr.2011.03.011

De Grave, J., Glorie, S., Buslov, M. M., Stockli, D. F., McWilliams, M. O., Batalev, V. Y., & Van den haute, P. (2013). Thermo-tectonic history of the Issyk-Kul basement (Kyrgyz Northern Tien Shan, Central Asia). *Gondwana Research*, *23*(3), 998–1020. https://doi.org/10.1016/j.gr.2012.06.014

Dzhalilov, M. R., Alekseev, M. N., Andreev, Y. N., & Salibaev, G. K. (1982). Mesozoic and Cenozoic deposits of the northern part of the Afghano-Tajik basin. In *Stratigraphic correlation between sedimentary basins of the ESCAP region, United Nations mineral resources development series* (Vol. III, pp. 131–137).

Dzhalilov, M. R., Andreev, Y. N., Khakimov, F. H., & Goltman, E. V. (1971). *Cretaceous sedimentary rocks in Central Tajikistan*. Donish. (in Russian).

Engdahl, E. R., Di Giacomo, D., Sakarya, B., Gkarlaouni, C. G., Harris, J., & Storchak, D. A. (2020). ISC-EHB 1964–2016, an improved data set for studies of Earth structure and global seismicity. *Earth and Space Science*, *7*(1). https://doi.org/10.1029/2019EA000897

Erslev, E. A. (1991). Trishear fault-propagation folding. *Geology*, *19*(6), 617–620. https://doi.org/10.1130/0091-7613(1991)019<0617:TFPF>2.3.CO;2

Feld, C., Haberland, C., Schurr, B., Sippl, C., Wetzel, H. U., Roessner, S., et al. (2015). Seismotectonic study of the Fergana Region (Southern Kyrgyzstan): Distribution and kinematics of local seismicity Seismology. *Earth Planets and Space*, *67*(1), 40. https://doi.org/10.1186/s40623-015-0195-1

Fürsich, F. T., Brunet, M. F., Auxiètre, J. L., & Munsch, H. (2017). Lower-Middle Jurassic facies patterns in the NW Afghan-Tajik Basin of southern Uzbekistan and their geodynamic context. *Geological Society, London, Special Publications*, *427*(1), 357–409. https://doi.org/10.1144/SP427.9

Gągała, Ł., Ratschbacher, L., Ringenbach, J. C., Kufner, S.-K., Schurr, B., Dedow, R., et al. (2020). Tajik basin and southwestern Tian Shan, northwestern India-Asia collision zone: 1. Structure, kinematics, and salt tectonics in the Tajik fold-and-thrust belt of the western foreland of the Pamir. *Tectonics*, *39*(5). https://doi.org/10.1029/2019TC005871

Gapais, D., Cobbold, P. R., Bourgeois, O., Rouby, D., & De Urreiztieta, M. (2000). Tectonic significance of fault-slip data. *Journal of Structural Geology*, *22*(7), 881–888. https://doi.org/10.1016/S0191-8141(00)00015-8

Glorie, S., & De Grave, J. (2016). Exhuming the Meso-Cenozoic Kyrgyz Tianshan and Siberian Altai-Sayan: A review based on low-temperature thermochronology. *Geoscience Frontiers*, *7*(2), 155–170. https://doi.org/10.1016/j.gsf.2015.04.003

Glorie, S., De Grave, J., Buslov, M. M., Zhimulev, F. I., Stockli, D. F., Batalev, V. Y., et al. (2011). Tectonic history of the Kyrgyz South Tien Shan (Atbashi-Inylchek) suture zone: The role of inherited structures during deformation-propagation. *Tectonics*, *30*(6). https://doi.org/10.1029/2011TC002949

Goode, J. K., Burbank, D. W., & Ormukov, C. (2014). Pliocene-Pleistocene initiation, style, and sequencing of deformation in the central Tien Shan. *Tectonics*, *33*(4), 464–484. https://doi.org/10.1002/2013TC003394

Havenith, H. B., Strom, A., Torgoev, I., Torgoev, A., Lamair, L., Ischuk, A., & Abdrakhmatov, K. (2015). Tien Shan geohazards database: Earthquakes and landslides. *Geomorphology*, *249*, 16–31. https://doi.org/10.1016/j.geomorph.2015.01.037

Heermance, R. V., Chen, J., Burbank, D. W., & Miao, J. (2008). Temporal constraints and pulsed Late Cenozoic deformation during the structural disruption of the active Kashi foreland, northwest China. *Tectonics*, *27*(6). https://doi.org/10.1029/2007TC002226

Huangfu, P., Li, Z. H., Zhang, K. J., Fan, W., Zhao, J., & Shi, Y. (2021). India-Tarim lithospheric mantle collision beneath western Tibet controls the Cenozoic building of Tian Shan. *Geophysical Research Letters*, *48*(14). https://doi.org/10.1029/2021GL094561

Ischuk, A., Bendick, R., Rybin, A., Molnar, P., Khan, S. F., Kuzikov, S., et al. (2013). Kinematics of the Pamir and Hindu Kush regions from GPS geodesy. *Journal of Geophysical Research: Solid Earth*, *118*(5), 2408–2416. https://doi.org/10.1002/jgrb.50185

Jia, Y., Fu, B., Jolivet, M., & Zheng, S. (2015). Cenozoic tectono-geomorphological growth of the SW Chinese Tian Shan: Insight from AFT and detrital zircon U-Pb data. *Journal of Asian Earth Sciences*, *111*, 395–413. https://doi.org/10.1016/j.jseaes.2015.06.023

Kaya, M. Y., Dupont-Nivet, G., Proust, J.-N., Roperch, P., Bougeois, L., Meijer, N., et al. (2019). Paleogene evolution and demise of the proto-Paratethys Sea in Central Asia (Tarim and Tajik basins): Role of intensified tectonic activity at ca. 41 Ma. *Basin Research*, *31*(3), 461–486. https://doi.org/10.1111/bre.12330

Kaya, M. Y., Dupont-Nivet, G., Proust, J. N., Roperch, P., Meijer, N., Frieling, J., et al. (2020). Cretaceous evolution of the Central Asian Proto-Paratethys Sea: Tectonic, eustatic, and climatic controls. *Tectonics*, *39*(9). https://doi.org/10.1029/2019TC005983

Kazakov, Y. M., Kreydenkov, G. P., Mamontov, A. N., Tadzhibekov, M., & Khasanov, A. K. (2002). *Textbook on geological practice in the Ziddy Basin*. Dushanbe. (in Russian).: Retrieved from https://nikzdaru.com/ziddi/text_ziddi.htm

Käßner, A., Ratschbacher, L., Jonckheere, R., Enkelmann, E., Khan, J., Sonntag, B.-L., et al. (2016). Cenozoic intracontinental deformation and exhumation at the northwestern tip of the India-Asia collision—Southwestern Tian Shan, Tajikistan, and Kyrgyzstan. *Tectonics*, *35*(9), 2171–2194. https://doi.org/10.1002/2015TC003897

Käßner, A., Ratschbacher, L., Pfänder, J. A., Hacker, B. R., Zack, G., Sonntag, B.-L., et al. (2017). Proterozoic-Mesozoic history of the Central Asian orogenic belt in the Tajik and southwestern Kyrgyz Tian Shan: U-Pb, $^{40}Ar/^{39}Ar$, and fission-track geochronology and geochemistry of granitoids. *Bulletin of the Geological Society of America*, *129*(3–4), 281–303. https://doi.org/10.1130/B31466.1

Klebelsberg, R. v. (1922). Beiträge zur Geologie Westturkestans. In *Ergebnisse der Expedition des Deutschen und Österreichischen Alpenvereins im Jahre 1913* (p. 488). Universitätsverlag Wagner. (in German).

Kley, J., Sobel, E. R., Voigt, T., Rembe, J., & Thiede, R. (2023). *Kinematics of the Pamir orogeny on a lithospheric scale*. EGU General Assembly 2023. EGU23-14406. https://doi.org/10.5194/egusphere-egu23-14406

Klocke, M., Voigt, T., Kley, J., Pfeifer, S., Rocktäschel, T., Keil, S., & Gaupp, R. (2017). Cenozoic evolution of the Pamir and Tien Shan mountains reflected in syntectonic deposits of the Tajik Basin. *Geological Society, London, Special Publications*, *427*(1), 523–564. https://doi.org/10.1144/SP427.7

Konopelko, D., Seltmann, R., Mamadjanov, Y., Romer, R. L., Rojas-Agramonte, Y., Jeffries, T., et al. (2017). A geotraverse across two paleo-subduction zones in Tien Shan, Tajikistan. *Gondwana Research*, *47*, 110–130. https://doi.org/10.1016/j.gr.2016.09.010

Kröner, A., Kovach, V., Belousova, E., Hegner, E., Armstrong, R., Dolgopolova, A., et al. (2014). Reassessment of continental growth during the accretionary history of the Central Asian Orogenic Belt. *Gondwana Research*, *25*(1), 103–125. https://doi.org/10.1016/j.gr.2012.12.023

Krymholts, G. Y., Mesezhnikov, M. S., Westermann, G. E. G., & Vassiljeva, T. I. (1988). The Jurassic ammonite zones of the Soviet Union. *Geological Society of America, Special Papers*, 1–3. https://doi.org/10.1130/SPE223

Kudriavtseva, A., Codilean, A. T., Sobel, E. R., Landgraf, A., Fülöp, R. H., Dzhumabaeva, A., et al. (2023). Impact of Quaternary glaciations on denudation rates in North Pamir—Tian Shan inferred from cosmogenic ^{10}Be and low-temperature thermochronology. *Journal of Geophysical Research: Earth Surface*, *128*(12). https://doi.org/10.1029/2023JF007193

Kufner, S.-K., Eken, T., Tilmann, F., Schurr, B., Yuan, X., Mechie, J., et al. (2018). Seismic anisotropy beneath the Pamir and the Hindu Kush: Evidence for contributions from crust, mantle lithosphere, and asthenosphere. *Journal of Geophysical Research: Solid Earth*, *123*(12), 10727–10748. https://doi.org/10.1029/2018JB015926

Kufner, S.-K., Schurr, B., Haberland, C., Zhang, Y., Saul, J., Ischuk, A., & Oimahmadov, I. (2017). Zooming into the Hindu Kush slab break-off: A rare glimpse on the terminal stage of subduction. *Earth and Planetary Science Letters*, *461*, 127–140. https://doi.org/10.1016/j.epsl.2016.12.043

Kufner, S.-K., Schurr, B., Ratschbacher, L., Murodkulov, S., Abdulhameed, S., Ischuk, A., et al. (2018). Seismotectonics of the Tajik Basin and surrounding mountain ranges. *Tectonics*, *37*(8), 2404–2424. https://doi.org/10.1029/2017TC004812

Kufner, S.-K., Schurr, B., Sippl, C., Yuan, X., Ratschbacher, L., Akbar, A. s. M., et al. (2016). Deep India meets deep Asia: Lithospheric indentation, delamination and break-off under Pamir and Hindu Kush (Central Asia). *Earth and Planetary Science Letters*, *435*, 171–184. https://doi.org/10.1016/j.epsl.2015.11.046

Lan, X., & Wei, J. (1995). *Late Cretaceous–early Tertiary marine bivalve fauna from the western Tarim Basin*. Chinese Science House.

Leonov, M. G. (2005). The post-oceanic geodynamics of the South Tien Shan region. *Russian Journal of Earth Sciences*, *7*(6), 1–27. https://doi.org/10.2205/2005ES000187

Li, L., Dupont-Nivet, G., Najman, Y., Kaya, M., Meijer, N., Poujol, M., & Aminov, J. (2022). Middle to late Miocene growth of the North Pamir. *Basin Research*, *34*(2), 533–554. https://doi.org/10.1111/bre.12629

Li, T., Chen, Z., Chen, J., Thompson Jobe, J. A., Burbank, D. W., Li, Z., et al. (2019). Along-strike and downdip segmentation of the Pamir Frontal Thrust and its association with the 1985 Mw 6.9 Wuqia earthquake. *Journal of Geophysical Research: Solid Earth*, *124*(9), 9890–9919. https://doi.org/10.1029/2019JB017319

Li, W., Chen, Y., Yuan, X., Xiao, W., & Windley, B. F. (2022). Intracontinental deformation of the Tianshan Orogen in response to India-Asia collision. *Nature Communications*, *13*(1), 3738. https://doi.org/10.1038/s41467-022-30795-6

Macaulay, E. A., Sobel, E. R., Mikolaichuk, A., Kohn, B., & Stuart, F. M. (2014). Cenozoic deformation and exhumation history of the Central Kyrgyz Tien Shan. *Tectonics*, *33*(2), 135–165. https://doi.org/10.1002/2013TC003376

Macaulay, E. A., Sobel, E. R., Mikolaichuk, A., Landgraf, A., Kohn, B., & Stuart, F. (2013). Thermochronologic insight into late Cenozoic deformation in the basement-cored Terskey Range, Kyrgyz Tien Shan. *Tectonics*, *32*(3), 487–500. https://doi.org/10.1002/tect.20040

McNab, F., Sloan, R. A., & Walker, R. T. (2019). Simultaneous orthogonal shortening in the Afghan-Tajik Depression. *Geology*, *47*(9), 862–866. https://doi.org/10.1130/G46090.1

Metzger, S., Gągała, Ł., Ratschbacher, L., Lazecký, M., Maghsoudi, Y., & Schurr, B. (2021). Tajik Depression and Greater Pamir neotectonics from InSAR rate maps. *Journal of Geophysical Research: Solid Earth*, *126*(12). https://doi.org/10.1029/2021JB022775

Metzger, S., Ischuk, A., Deng, Z., Ratschbacher, L., Perry, M., Kufner, S. K., et al. (2020). Dense GNSS profiles across the northwestern tip of the India-Asia collision zone: Triggered slip and westward flow of the Peter the First Range, Pamir, into the Tajik Depression. *Tectonics*, *39*(2), e2019TC005797. https://doi.org/10.1029/2019TC005797

Mohadjer, S., Bendick, R., Ischuk, A., Kuzikov, S., Kostuk, A., Saydullaev, U., et al. (2010). Partitioning of India-Eurasia convergence in the Pamir-Hindu Kush from GPS measurements. *Geophysical Research Letters*, *37*(4). https://doi.org/10.1029/2009GL041737

Molnar, P., & Stock, J. M. (2009). Slowing of India's convergence with Eurasia since 20 Ma and its implications for Tibetan mantle dynamics. *Tectonics*, *28*(3). https://doi.org/10.1029/2008TC002271

Mordvintsev, D., Barrier, E., Brunet, M. F., Blanpied, C., & Sidorova, I. (2017). Structure and evolution of the Bukhara-Khiva region during the Mesozoic: The northern margin of the Amu-Darya Basin (southern Uzbekistan). *Geological Society, London, Special Publications*, *427*(1), 145–174. https://doi.org/10.1144/SP427.16

Morin, J., Jolivet, M., Barrier, L., Laborde, A., Li, H., & Dauteuil, O. (2019). Planation surfaces of the Tian Shan Range (Central Asia): Insight on several 100 million years of topographic evolution. *Journal of Asian Earth Sciences*, *177*, 52–65. https://doi.org/10.1016/j.jseaes.2019.03.011

Morin, J., Jolivet, M., Robin, C., Heilbronn, G., Barrier, L., Bourquin, S., & Jia, Y. (2018). Jurassic paleogeography of the Tian Shan: An evolution driven by far-field tectonics and climate. *Earth-Science Reviews*, *187*, 286–313. https://doi.org/10.1016/j.earscirev.2018.10.007

Morin, J., Jolivet, M., Shaw, D., Bourquin, S., & Bataleva, E. (2021). New sedimentological and palynological data from the Yarkand-Fergana Basin (Kyrgyz Tian Shan): Insights on its Mesozoic paleogeographic and tectonic evolution. *Geoscience Frontiers*, *12*(1), 183–202. https://doi.org/10.1016/j.gsf.2020.04.010

Nesmeyanov, C. A., & Barkhatov, I. I. (1978). The recent and earthquake generating structural features in the western Gissar-Alai region. Moscow. (in Russian).

Nikolaev, V. G. (2002). Afghan-Tajik depression: Architecture of sedimentary cover and evolution. *Russian Journal of Earth Sciences*, *4*(6), 399–421. https://doi.org/10.2205/2002ES000106

Perry, M., Kakar, N., Ischuk, A., Metzger, S., Bendick, R., Molnar, P., & Mohadjer, S. (2019). Little geodetic evidence for localized Indian subduction in the Pamir-Hindu Kush of Central Asia. *Geophysical Research Letters*, *46*(1), 109–118. https://doi.org/10.1029/2018GL080065

Pieri, M., Kunze, K., Burlini, L., Stretton, I., Olgaard, D. L., Burg, J.-P., & Wenk, H.-R. (2001). Texture development of calcite by deformation and dynamic recrystallization at 1000 K during torsion experiments of marble to large strains. *Tectonophysics*, *330*(1–2), 119–140. https://doi.org/10.1016/S0040-1951(00)00225-0

Portnyagin, E. A., Koshlakov, G. V., & Kuznetsov, Y. S. (1976). Problem of mutual relationships between the deep-seated Paleozoic structures of Southern Tien Shan and the buried Tadzhik-Afghan Massif. *International Geology Review*, *18*(4), 450–454. https://doi.org/10.1080/00206817609471226

Przhiyalgovskii, E. S., & Lavrushina, E. V. (2020). The structures of the Alai and Kichi-Karakol depressions and the latest deformations in their mountainous surroundings (Southern Tian Shan). *Lithosphere*, *20*(6), 771–790. (in Russian). https://doi.org/10.24930/1681-9004-2020-20-6-771-790

Rai, S. S., Priestley, K., Gaur, V. K., Mitra, S., Singh, M. P., & Searle, M. (2006). Configuration of the Indian Moho beneath the NW Himalaya and Ladakh. *Geophysical Research Letters*, *33*(15). https://doi.org/10.1029/2006GL026076

Ratschbacher, L., Wenk, H.-R., & Sintubin, M. (1991). Calcite textures: Examples from nappes with strain-path partitioning. *Journal of Structural Geology*, *13*(4), 369–384. https://doi.org/10.1016/0191-8141(91)90011-7

Rey, P. F., Teyssier, C., & Whitney, D. L. (2010). Limit of channel flow in orogenic plateaux. *Lithosphere*, *2*(5), 328–332. https://doi.org/10.1130/L114.1

Robert, A. M. M., Fernandez, M., Jiménez-Munt, I., & Vergés, J. (2017). Lithospheric structure in Central Eurasia derived from elevation, geoid anomaly and thermal analysis. *Geological Society, London, Special Publications*, *427*(1), 271–293. https://doi.org/10.1144/SP427.10

Rogozhin, E. A. (2004). Morphology and origin of folding in the South Tien Shan. *Russian Journal of Earth Sciences*, *6*(1), 1–34. https://doi.org/10.2205/2004ES000142

Rolland, Y., Jourdon, A., Petit, C., Bellahsen, N., Loury, C., Sobel, E. R., & Glodny, J. (2020). Thermochronology of the highest central Asian massifs (Khan Tengri - Pobedi, SE Kyrgyztan): Evidence for Late Miocene (ca. 8 Ma) reactivation of Permian faults and insights into building the Tian Shan. *Journal of Asian Earth Sciences*, *200*, 104466. https://doi.org/10.1016/j.jseaes.2020.104466

Roud, S. C., Wack, M. R., Gilder, S. A., Kudriavtseva, A., & Sobel, E. R. (2021). Miocene to early Pleistocene depositional history and tectonic evolution of the Issyk-Kul Basin, Central Tian Shan. *Geochemistry, Geophysics, Geosystems*, *22*(4). https://doi.org/10.1029/2020GC009556

Schneider, F. M., Yuan, X., Schurr, B., Mechie, J., Sippl, C., Kufner, S.-K., et al. (2019). The crust in the Pamir: Insights from receiver functions. *Journal of Geophysical Research: Solid Earth*, *124*(8), 9313–9331. https://doi.org/10.1029/2019JB017765

Schurr, B., Ratschbacher, L., Sippl, C., Gloaguen, R., Yuan, X., & Mechie, J. (2014). Seismotectonics of the Pamir. *Tectonics*, *33*(8), 1501–1518. https://doi.org/10.1002/2014TC003576

Seeber, L., & Sorlien, C. C. (2000). Listric thrusts in the western Transverse Ranges, California. *GSA Bulletin*, *112*(7), 1067–1079. https://doi.org/10.1130/0016-7606(2000)112<1067:ltitwt>2.0.co;2

Şengör, A. M. C., Natal'in, B. A., & Burtman, V. S. (1993). Evolution of the Altaid tectonic collage and Palaeozoic crustal growth in Eurasia. *Nature*, *364*(6435), 299–307. https://doi.org/10.1038/364299a0

Shcherba, I. G. (1990). The reflection of the Alpine tectonic phases in the Mz-Kz rocks of the South Tien Shan region. *Geotectonics*, *23*(2), 42–60. (in Russian).

Sippl, C., Ratschbacher, L., Schurr, B., Krumbiegel, C., Rui, H., Pingren, L., & Abdybachaev, U. (2014). The 2008 Nura earthquake sequence at the Pamir-Tian Shan collision zone, southern Kyrgyzstan. *Tectonics*, *33*(12), 2382–2399. https://doi.org/10.1002/2014TC003705

Sippl, C., Schurr, B., Yuan, X., Mechie, J., Schneider, F. M., Gadoev, M., et al. (2013). Geometry of the Pamir-Hindu Kush intermediate-depth earthquake zone from local seismic data. *Journal of Geophysical Research: Solid Earth*, *118*(4), 1438–1457. https://doi.org/10.1002/jgrb.50128

Sobel, E. R., Oskin, M., Burbank, D., & Mikolaichuk, A. (2006). Exhumation of basement-cored uplifts: Example of the Kyrgyz Range quantified with apatite fission track thermochronology. *Tectonics*, *25*(2). https://doi.org/10.1029/2005TC001809

Spang, J. H. (1972). Numerical method for dynamic analysis of calcite twin lamellae. *Geological Society of America Bulletin*, *83*(2), 467–472. https://doi.org/10.1130/0016-7606(1972)83[467:NMFDAO]2.0.CO;2

Sperner, B., & Ratschbacher, L. (1994). A Turbo Pascal program package for graphical presentation and stress analysis of calcite deformation. *Zeitschrift der Deutschen Geologischen Gesellschaft*, *145*, 414–423.

Steffen, R., Steffen, H., & Jentzsch, G. (2011). A three-dimensional Moho depth model for the Tien Shan from EGM2008 gravity data. *Tectonics*, *30*(5). https://doi.org/10.1029/2011TC002886

Stübner, K., Ratschbacher, L., Rutte, D., Stanek, K., Minaev, V., Wiesinger, M., & Gloaguen, R. (2013). The giant Shakhdara migmatitic gneiss dome, Pamir, India-Asia collision zone: 1. Geometry and kinematics. *Tectonics*, *32*(4), 948–979. https://doi.org/10.1002/tect.20057

Tang, T., Yang, H., Lan, X., Yu, C., Xue, Y., Zhang, Y., et al. (1989). *Marine late Cretaceous and early Tertiary stratigraphy and petroleum geology in western Tarim Basin, China*. Science Press.

Thomas, J. C., Perroud, H., Cobbold, P. R., Bazhenov, M. L., Burtman, V. S., Chauvin, A., & Sadybakasov, E. (1993). A paleomagnetic study of Tertiary formations from the Kyrgyz Tien-Shan and its tectonic implications. *Journal of Geophysical Research*, *98*(B6), 9571–9589. https://doi.org/10.1029/92JB02912

Thompson, S. C., Weldon, R. J., Rubin, C. M., Abdrakhmatov, K., Molnar, P., & Berger, G. W. (2002). Late Quaternary slip rates across the central Tien Shan, Kyrgyzstan, central Asia. *Journal of Geophysical Research*, *107*(B9). ETG 7-1–ETG 7-32. https://doi.org/10.1029/2001jb000596

Trilsch, F., Ratschbacher, L., Vergés, J. M., Nakapelyukh, M., Schurr, B., & Gadoev, M. (2025). Structural geologic maps, field data and outcrop images from Cenozoic intra-montane basins in the southwestern Tian Shan [Dataset]. *GFZ Data Services*. https://doi.org/10.5880/fidgeo.2025.001

Trilsch, F., Reuter, S., Ratschbacher, L., Jonckheere, R., Härtel, B., Jafari Ansari, S., et al. (2025). Southwestern Tian Shan: 2. Timing of Cenozoic mountain building, intra-montane basin inversion, and relation to lithospheric mantle indentation. *Tectonics*, *44*, e2024TC008491. https://doi.org/10.1029/2024TC008491

Twiss, R. J. (2009). An asymmetric micropolar moment tensor derived from a discrete-block model for a rotating granular substructure. *Bulletin of the Seismological Society of America*, *99*(2B), 1103–1131. https://doi.org/10.1785/0120080084

Twiss, R. J., & Unruh, J. R. (1998). Analysis of fault slip inversions: Do they constrain stress or strain rate? *Journal of Geophysical Research*, *103*(B6), 12205–12222. https://doi.org/10.1029/98jb00612

Volkova, N. I., & Budanov, V. I. (1999). Geochemical discrimination of metabasalt rocks of the Fan-Karategin transitional blueschist/greenschist belt, South Tianshan, Tajikistan: Seamount volcanism and accretionary tectonics. *Lithos*, *47*(3–4), 201–216. https://doi.org/10.1016/S0024-4937(99)00019-5

Wang, X., Carrapa, B., Chapman, J. B., Henriquez, S., Wang, M., DeCelles, P. G., et al. (2019). Paratethys last gasp in Central Asia and Late Oligocene accelerated uplift of the Pamirs. *Geophysical Research Letters*, *46*(21), 11773–11781. https://doi.org/10.1029/2019GL084838

Windley, B. F., Alexeiev, D., Xiao, W., Kröner, A., & Badarch, G. (2007). Tectonic models for accretion of the Central Asian Orogenic Belt. *Journal of the Geological Society*, *164*(1), 31–47. https://doi.org/10.1144/0016-76492006-022

Worthington, J. R., Kapp, P., Minaev, V., Chapman, J. B., Mazdab, F. K., Ducea, M. N., et al. (2017). Birth, life, and demise of the Andean–syn-collisional Gissar arc: Late Paleozoic tectono-magmatic-metamorphic evolution of the southwestern Tian Shan, Tajikistan. *Tectonics*, *36*(10), 1861–1912. https://doi.org/10.1002/2016TC004285

Yang, W., Jolivet, M., Dupont-Nivet, G., & Guo, Z. (2014). Mesozoic - Cenozoic tectonic evolution of southwestern Tian Shan: Evidence from detrital zircon U/Pb and apatite fission track ages of the Ulugqat area, Northwest China. *Gondwana Research*, *26*(3–4), 986–1008. https://doi.org/10.1016/j.gr.2013.07.020

Yin, A., Nie, S., Craig, P., Harrison, T. M., Ryerson, F. J., Xianglin, Q., & Geng, Y. (1998). Late Cenozoic tectonic evolution of the southern Chinese Tian Shan. *Tectonics*, *17*(1), 1–27. https://doi.org/10.1029/97TC03140

Zhao, J., Yuan, X., Liu, H., Kumar, P., Pei, S., Kind, R., et al. (2010). The boundary between the Indian and Asian tectonic plates below Tibet. *Proceedings of the National Academy of Sciences of the United States of America*, *107*(25), 11229–11233. https://doi.org/10.1073/pnas.1001921107

Zubovich, A., Schöne, T., Metzger, S., Mosienko, O., Mukhamediev, S., Sharshebaev, A., & Zech, C. (2016). Tectonic interaction between the Pamir and Tien Shan observed by GPS. *Tectonics*, *35*(2), 283–292. https://doi.org/10.1002/2015TC004055

Zubovich, A., Wang, X. Q., Scherba, Y. G., Schelochkov, G. G., Reilinger, R., Reigber, C., et al. (2010). GPS velocity field for the Tien Shan and surrounding regions. *Tectonics*, *29*(6). https://doi.org/10.1029/2010TC002772

References From the Supporting Information

Bande, A., Radjabov, S., Sobel, E. R., & Sim, T. (2017). Cenozoic palaeoenvironmental and tectonic controls on the evolution of the northern Fergana Basin. *Geological Society, London, Special Publications*, *427*(1), 313–335. https://doi.org/10.1144/SP427.12

Golikov, A. N., Pyatkov, K. K., & Posokhova, M. M. (1966). 1:200,000 map series, Sheet J-42-III geological survey of the CCCP.